INTERACTIONS IN CATION PERMEATION THROUGH THE GRAMICIDIN CHANNEL

Cs, Rb, K, Na, Li, Tl, H, and Effects of Anion Binding

GEORGE EISENMAN, *Department of Physiology, University of California at Los Angeles Medical School, Los Angeles, California 90024 U.S.A.*
JOHN SANDBLOM, *Department of Physiology and Medical Biophysics, Biomedical Center, Uppsala, Sweden, and*
ERWIN NEHER, *Max-Planck-Institut für Biophysikalische Chemie, Göttingen, West Germany*

ABSTRACT As a prototype for binding and interaction in biological Na and K channels, the single channel conductances for Li, Na, K, Rb, Cs, H, and Tl and the membrane potentials for Tl-K mixtures are characterized for gramicidin A over wider concentration ranges than previously and analyzed using an "equilibrium domain" model that assumes a central rate-determining barrier. Peculiarities in the conductance-concentration relationship for TlF, $TlNO_3$, and TlAc suggest that anions bind to Tl-loaded channels, and the theory is extended to allow for this. For concreteness, the selectivity of cation permeation is characterized in terms of individual binding and rate constants of this model, with the conclusions that the strongest site binds Cs>Rb>K>Na>Li, while the next strongest binds Na>K>Li>Rb>Cs. However, because Schagina, Grinfeldt, and Lev's recent finding of single filing (personal communication) indicates that the channel sites in gramicidin cannot be at equilibrium with the solution, and work in progress with Hägglund and Enos (*Biophys. J.* **21**:26*a*. [Abstr.]) indicates that the simplest model adequate to account for the observed concentration-dependences of flux-ratio, conductance, *I–V* characteristic, and permeability has three barriers and four sites, some implications of additional rate-determining barriers at the mouth of the channel are discussed. The results are summarized using phenomenological, "experimental" parameters that provide a model-independent way to represent the data concisely and which can be interpreted physically in terms of any desired model.

INTRODUCTION AND BACKGROUND

As a model for multi-ion occupancy of biological channels, this paper will describe the complicated conductance-concentration behavior as well as the observed concentration dependence of permeability ratios characteristic of a particularly simple poly-

This paper was presented in the Symposium "Ionic Motion and Gating in Biological and Artificial Channels." at the 21st Annual Meeting of the Biophysical Society, 18 Feb 1977, New Orleans, La.

peptide channel, that of the dimer of the neutral pentadecapeptide, gramicidin A (Urry, 1971; Hladky and Haydon, 1970, 1972; Läuger, 1973). We then analyze the observed complexities as the theoretically expected consequences (Sandblom, et al., 1977) of simultaneous occupancy of the gramicidin channel by more then one cation. We here extend our description beyond the previously characterized Tl^+ and K^+ species (Eisenman, et al. 1977) to the conductances seen for Cs^+, Rb^+, Na^+, Li^+, and H^+, for all of which we find our previously developed theory to be adequate. We also describe and characterize certain small, but not negligible, effects of different anions seen with Tl^+-loaded channels, which we will interpret by extension of our previous theory to be a consequence of a secondary binding of anions to cation-loaded channels. In so doing we examine some biologically interesting consequences of the possibility that anions could bind near the mouth of a cation-occupied channel and, through essentially electrostatic interactions, alter the permeation properties for cations. We will not consider here in detail such important additional concentration-dependent behaviors as the deviations from the simple Ussing flux-ratio relationship for unidirectional ^{86}Rb fluxes recently described by Schagina, Grinfeldt, and Lev (personal communication) or the well-known concentration-dependence of the conductance-voltage characteristic (Hladky and Haydon, 1972; Läuger, 1973). Schagina, Grinfeldt, and Lev find the unidirectional flux ratio of ^{86}Rb to depend on the second power of the electrochemical activity ratio over the concentration range 0.001–0.1 M RbCl, which implies that Rb^+ ions move as pairs over this entire concentration range. These two sets of results, together with the RbCl conductance-concentration data of the present paper, suffice to narrow considerably the choice of acceptable single-filing models (Hägglund et al., 1978). In particular, the pairwise movement implied by Lev's important flux ratio findings will require modification of the simplifying assumption we have made in all our work to date that equilibrium exists between all channel sites and the aqueous solution. For simplicity, we will continue to make this assumption in extending the theory to include anion effects, because the general features of anion effects are clearly illustrated thereby; it would be premature to try to use a model with more kinetic details before these have been worked out for cation permeation in the absence of anion effects, an area now receiving intense attention (Levitt, 1978; Hladky, et al., 1978; Hägglund et al., 1978) in theoretical treatments based on Heckmann-Chizmadjev-Eyring single-filing models (Heckmann, 1972; Heckmann and Vollmerhaus, 1970; Heckmann et al., 1972; Chizmadjev and Aityan, 1974, 1977).

We are comfortable in using such an oversimplication because we have recently found (Hägglund et al., 1978) that a "translation" between various models (e.g. one-barrier, four-site; three-barrier, four-site; and even three-barrier, two-site) is possible at least for the conductance-concentration behavior when the data are characterized in terms of phenomenological "experimental" rate constants and binding constants suggested by analogy between conventional enzyme kinetics and the formal properties of the one-barrier, four-site "equilibrium domain" model. However, because one of the purposes of this paper is to give some sense of perspective, we will discuss briefly the implications of taking additional barriers into account, relying upon work in

progress with Hägglund and Enos, which indicates that the simplest model adequate to account for the observed concentration-dependences of flux-ratio, conductance, I–V characteristic, and permeability has three barriers and four sites (Hägglund et al., 1978).

This paper is intended to be speculative and provocative. The work is in an early stage and some of the results must still be regarded as preliminary. While we could have ignored anion effects in comparing our data with theory, we did not do so because we felt it would be instructive to consider what anion binding could do to cation permeation as a general question, as well as to provide some estimate of the magnitude of anion effects on cation permeation in the gramicidin channel. At this point in developing a more microscopic understanding of ion permeation in channels, it is probably more important to examine first what could happen in a relatively simple multi-ion model before becoming too concerned with what actually does happen in the gramicidin channel.

This paper is concerned with the electrical signs of interactions among ions in channels. Interactions imply occupancy by more than one ion, and the phenomena to be expected in a multiply-occupiable channel can be even more complex than those already described (Hille, 1975) for one-ion-occupiable channels. Even without the possibility of interactions resulting from multiple occupancy, the selectivity of the simplest one-ion-occupiable channel as defined through membrane potentials by permeability will generally correspond to that defined by conductance only at the lowest concentrations. This lack of correspondence is because in saturating systems two coefficients, a binding constant and a rate constant (analogous to the Michaelis constant and maximal velocity), are necessary to define conductance (see below). In contrast, only one constant (the product of the binding constant and rate constant) is needed to define the permeability.

In the case of a more-than-one-ion-occupiable channel the permeability and conductance behavior can be dramatically affected by cation-cation interactions, which manifest themselves both as concentration-dependent permeability ratios (Eisenman et al., 1977; Sandblom et al., 1977) and as "anomalous mole-fraction dependent" conductances (Neher, 1975; Andersen, 1975; Neher et al., 1978), resembling similar phenomena in biological channels (Cahalan and Begenisich, 1976; Hagiwara and Takahashi, 1974). How this comes about will be clarified in Figs. 1 and 2, where we examine various conceivable energy profiles for cation permeation across the gramicidin channel and show how the rate constants and binding constants of these profiles will determine the conductance-concentration behavior in a way amenable to their measurement as model-independent "experimental" parameters given by certain intercepts and slopes on plots analogous to those used in classical enzyme kinetics.

The Energy Profile for Cation Permeation through the Gramicidin Channel

Fig. 1 schematizes the energy profile for cation permeation through a gramicidin channel, at the top presenting "realistic" profiles corresponding to two conceivable processes of dehydration, in one step at the left and in two steps at the right. Only

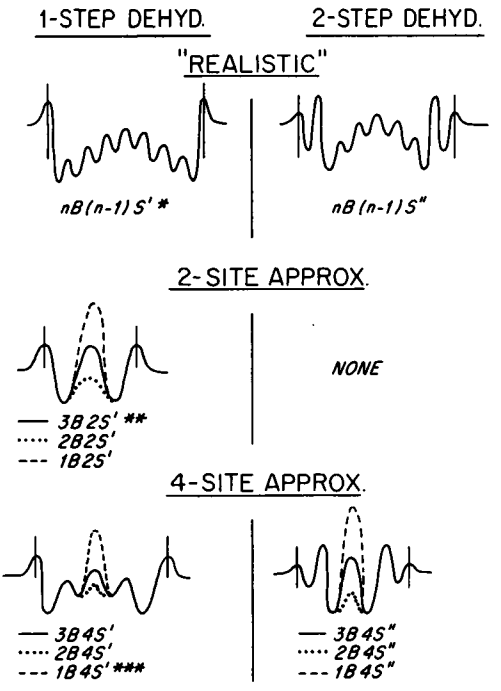

FIGURE 1 Classification of energy profiles for conceivable single-filing (series-site) models for the gramicidin A channel. The upper portion of the figure presents "realistic" profiles across the channel (membrane boundaries indicated by vertical lines) under conditions of one-step dehydration (left) and two-step dehydration (right). The "realistic" profiles are to be regarded as the result of a repulsive electrostatic image potential with its maximum at the center and a series of (uniform) barriers and wells within the gramicidin channel representing intrinsic attractive interactions with the ligands lining the wall of the channel (cf. Sandblom et al., 1977, Fig. 3). The wells represent energy minima for the ions, ligands, and H_2O molecules and include the conformational energy of the entire molecule, while the barriers represent less energetically favorable arrangements of all of these along the reaction (diffusion) coordinate. Previously examined models are designated by *(Läuger, 1973), **(Hladky, 1972), and ***(Sandblom et al., 1977).

energy profiles for unoccupied channels are indicated and, of course, shifts in these occur with loading (examples will be found in Fig. 13 and Fig. 2*d*). The wells in these profiles correspond to binding sites, and the various peaks correspond to activation energy barriers as in classical Eyring theory. Throughout this paper we will refer to the "peak-well" difference as the "barrier." All peaks and wells are referred to the reference state of the energy level of the permeant ion in the aqueous solution. The one-step dehydration process (* in Fig. 1) was essentially suggested by Läuger (1973), omitting the image force effect; but the two-step dehydration process needs a little description because it has not been considered previously. In this process, by analogy to the corresponding transition state for loading and unloading ion-carrier complexes (cf. Krasne and Eisenman, 1976, Fig. 13), we imagine that the first energy minimum occurs when an ion is half-hydrated and half-bound so that the first well is taken as halfway between the aqueous reference level and the level corresponding to its fully

bound (maximally dehydrated) state at the second energy minimum. If dehydration occurs in two steps, the highest barrier is likely to exist at the second step, because the major conformational energy change with analogous carriers occurs in the last steps of dehydration (Grell, 1975), and indeed this barrier should contain the activation energy for rearranging the conformation of the channel over its entire length. An important consequence of this essentially cooperative process is that all the remaining sites will then be in their optimal arrangement for binding the cation so that all other internal barriers are expected to be smaller than the barrier between the partially dehydrated and maximally dehydrated states.

The remainder of the figure classifies the various two-site and four-site approximations to these "realistic" cases for the indicated numbers of significantly rate-determining barriers (when any barrier exceeds the others sufficiently, it is the only rate-determining one). Using B to designate barriers and S to denote sites, and signifying one-step dehydration by ′ and two-step dehydration by ″, a convenient notation is developed. For example, 3B2S′ represents a three-barrier, two-site model with one-step dehydration of the type** in Fig. 1 first proposed by Hladky (1972), in his two-site lattice model. The "equilibrium domain" model of Sandblom et al., (1977), indicated by *** in Fig. 1, is the model used for the detailed theoretical interpretation in the present paper. However, in addition, we present the results using phenomenological, "experimental" parameters that provide a model-independent way to represent the data concisely, and which can subsequently be interpreted physically in terms of any desired model (e.g., Levitt, 1978; Hladky et al., 1978; Chizmadjev and Aityan, 1974, 1977).[1]

SINGLE CHANNEL CONDUCTANCES

We here describe the conductance-concentration behavior for Rb^+, Li^+, and H^+, as well as extending the concentration ranges for the previously characterized species Na^+, K^+, Cs^+, and Tl^+ (Hladky and Haydon, 1972; Eisenman et al. 1977). The data for RbCl are of particular interest, because they describe the conductance behavior of the channel over the concentration range where Lev's group have characterized single filing by tracer studies with ^{86}Rb. We also examine the effect of different anions, presenting our results as in Fig. 2 as plots of conductance (G) vs. conductance divided by ionic activity (G/a), analogous to an Eadie-Hofstee type of kinetic representation (Zeffren and Hall, 1973, p. 67) or to a Scatchard plot for equilibrium binding (Bull, 1964, p. 120).

The (Eadie-Hofstee Type) G vs. G/a Plot

In analyzing conductance-concentration (more precisely, activity) relationships in systems all of whose sites are in equilibrium with the aqueous solution (and even in those where some or all the sites are not in equilibrium) a plot of G vs. G/a is not only

[1] Hille, B., and W. Schwarz. 1978. K channels of nerve and muscle. Single-file, multi-ion pores. Manuscript in preparation.

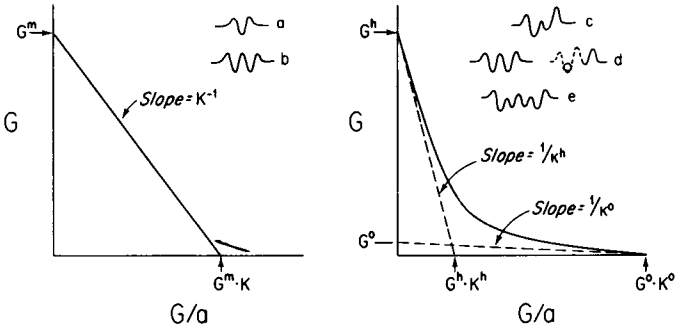

FIGURE 2 Schematic representation of Eadie-Hofstee type plot for conductance (G) vs. conductance/activity (G/a) for a channel with one class of sites (left) or two classes of sites (right). The values of the y-intercepts correspond to maximum limiting conductances and are analogous to the maximum velocity constants (V_{max}) of enzyme kinetics. The slopes are inversely proportional to the "experimental" binding constant (i.e. directly proportional to the Michaelis-Menten dissociation constant, k_m). Various energy profiles are indicated as inserts that could lead to this kind of behavior. For example, a channel with experimentally observed behavior like that at the left might correspond to profile *a* for one site or to profile *b* for two identical, noninteracting sites. The situations that would lead to behavior like that at the right could result from two initially different, noninteracting sites (*c*); two initially identical, interacting sites, the second of whose energy level changes on loading the first (*d*); or to two pairs of initially different, but noninteracting sites (*e*). Note that in all cases the slopes and intercepts of the Eadie-Hofstee type plots are characterized by a set of phenomenological "experimental" apparent rate constants and binding constants (G^m, K, and G^0,G^h, K^0, K^h, respectively), whose physical meaning can be assessed by reinterpreting them in terms of the corresponding "physical" rate constants and binding constants of a given model.

convenient, preserving the directly measured values of conductances, but also shows the separate contributions to selectivity of rate constants, binding constants, and their products (i.e., permeabilities). Thus the y-intercept on such a plot gives the maximum limiting rate, the slope gives the inverse binding constant, and the x-intercept gives the permeability (the product of the rate constant and the binding constant). The existence of more then one class of binding sites is also easily detected in such plots, because a one-site system yields a single straight line, whereas a two-site system yields a curve with two straight line segments, as illustrated at the left and right of Fig. 2, respectively (for simplicity blocking effects are ignored). The constants extracted from such a plot may be regarded as being phenomenological and will be designated as "experimental" throughout this paper. The more familiar Lineweaver-Burke-type plot yields the same information but is less convenient because one really needs to plot the data twice to examine both the high and low concentration behavior (a log-log plot of the Lineweaver-Burke type can avoid this difficulty, and is, of course, equivalent to a direct plot of log G vs. log a). The "experimental" parameters can be interpreted in terms of the physical parameters of a given model; and one such interpretation will be given here for the 1B4S′ model. Alternative interpretations have now been accomplished in terms of 3B2S′, 2B4S′, and 2B4S″ models and certain occupancy states of 3B4S′ and 3B4S″ models (Hägglund et al., 1978), and from these it it seems

likely that a "translation" can be made between the phenomenological "experimental" parameters and the appropriate "physical" rate constants and binding constants of any model of adequate complexity.

For the one-site case presented at the left of Fig. 2, the y-intercept G^m corresponds to the maximum conductance in the limit of high ion concentration (analogous to V_{max} in enzyme kinetics); the inverse slope is the binding constant K of the site ($1/k_m$ in enzyme kinetics). The x-intercept is the product ($G^m \cdot K$), which represents the permeability. From this plot it should be clear why even for a simple one-ion-saturable channel, as mentioned in the introduction, two separate constants (G^m and K) are needed to define the conductance; whereas one constant (the product $G^m \cdot K$) suffices to define the permeability. The inserts give examples of equivalent but physically different situations that would give rise to such behavior; a single site (*a*) and a pair of identical noninteracting sites (*b*) presented at the left of Fig. 2. For the two-site case presented at the right of Fig. 2, the plot is a curve with two straight line asymptotes whose intercepts and slopes correspond to the "experimental" binding constants (K^0, K^h); maximal "experimental" conductances (G^0, G^h); and their products ($G^0 \cdot K^0$, $G^h \cdot K^h$) at low and high concentrations, respectively. Note that each of the constants G, K, and ($G \cdot K$) would correspond to the appropriate levels of particular barriers, wells, and peaks of an Erying energy profile (cf. Hille, 1975, 277–285). The inserts give examples of physical situations that would lead to such behavior: two noninteracting sites of intrinsically different binding- (and rate-) constants (*c*); two initially identical, interacting sites (*d*); and two pairs of initially differing, noninteracting sites (*e*).

Salts of Li^+, Na^+, K^+, Rb^+, Cs^+, and H^+

Fig. 3 illustrates the single channel conductances of valine gramicidin A in glyceryl monooleate hexadecane bilayers measured for the chlorides of Li^+, Na^+, K^+, Rb^+, and Cs^+ (experimental details will be found in Neher et al., 1978, which also gives the data in tabular form and presents log-log plots of conductance vs. ionic activity which may interest those who find the Eadie-Hofstee-type representation to be opaque). Data for other anions are also given for K^+, Na^+, Li^+, and H^+. Our observations agree quite satisfactorily with previous results of others in the middle and high concentration regions for the same lipid (Hladky and Haydon, 1972; Bamberg et al. 1976) and are also consistent with those of Andersen (1978) in phosphatidyl ethanolamine decane membranes when suitable allowances for dipole potential differences are made (Andersen, unpublished; Eisenman, unpublished). What is new is our extension of the observations to lower concentrations than previously studied which produces the "foot" at the right seen most easily for Cs but also discernible for Rb, K, and H. This constitutes evidence for the existence of a previously undescribed additional binding site with a higher affinity for these species, which should be present for all cations to be consistent with our previous finding of such a site for Tl^+ and K^+ (Eisenman et al., 1977). Evidence that this "foot" is not artifactual and really represents an additional binding site comes from several sources: (*a*) from analysis of membrane potentials in Tl-K mixtures

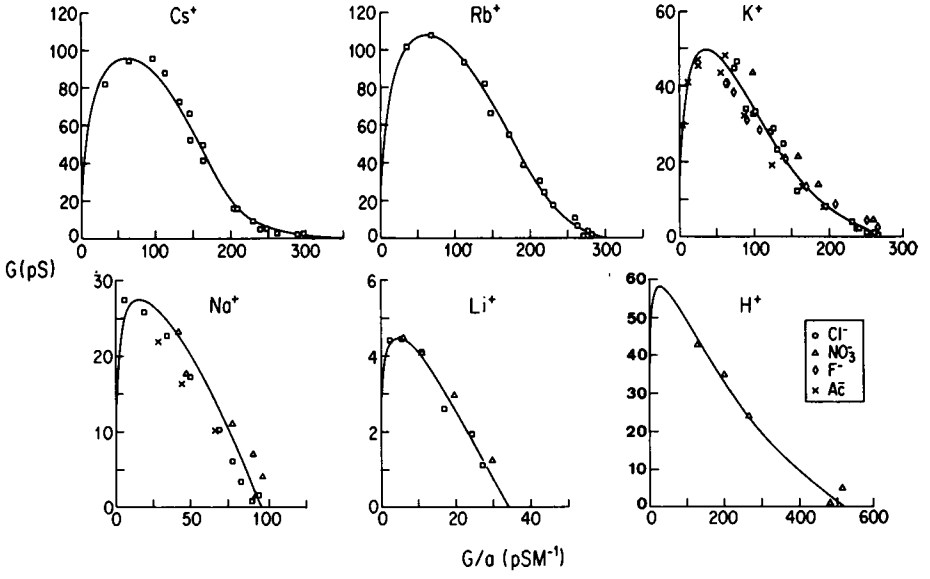

FIGURE 3 G vs. G/a (Eadie-Hofstee type) plot for the single channel conductances of the indicated cations (50 mV applied potential, GMO/hexadecane bilayers, valine gramicidin A for all conductances of this paper). Squares represent chlorides, triangles nitrates, diamonds fluoride, and crosses acetates. The theoretical curves have been drawn according to Eq. 3 with the parameters of Table I. Activity coefficient corrections assumed cation activity coefficients to be equal to tabulated values of the mean activity coefficients.

which showed a strong concentration-dependence of permeability ratios (Eisenman et al., 1977), (*b*) from Tl blocking effects on K^+ conductance (Sandblom et al., 1977); and (*c*) from controls eliminating possible surface charge effects described elsewhere (Neher, et al., 1978). The systematic behavior of K^0, K^h, G^0, and G^h for the five alkali cations, shown in Fig. 11, gives further support to this interpretation since it is reasonable to assume that the same process underlying the clearly prominent foot for Cs^+ and Tl^+ is present for other cations where the foot is less prominent.[2]

In all cases the experimental data points can be compared with theoretical curves drawn according to the expectations of our previously published model with the "experimental" parameters given in Table I. (The theoretical curves for the 1B4S′ model were drawn from Eq. 3 by using the translation of Table III to obtain the physical parameters of this model; such curves are of course identical to purely phenomenological curves drawn using the "experimental" parameters and the "translated" Eq. 3. Equally adequate theoretical curves are produced for other models (e.g. 3B2S′, 2B4S″,

[2] Furthermore, corresponding signs of several binding sites are seen in the more familiar, but far less convenient Lineweaver-Burke representation, as well as on log conductance vs. log activity plots. (The foot is difficult to see on linear plots of conductance vs. activity; but this is hardly surprising since such plots give almost no weight to the important conductance behavior at low ion concentrations).

TABLE I

"EXPERIMENTAL" PARAMETERS USED FOR FITTING CONDUCTANCE DATA IN SYMMETRICAL SINGLE SALT SOLUTIONS

	G^0	K^0	G^h	K^h	K^∞
	pS	M^{-1}	pS	M^{-1}	M^{-1}
Li^+*	3.8	9	4.0	1.2	0.03
Na^+*	4.9	20	36	2.0	0.1
K^+*	6.8	40.4	84.7	1.48	0.27
Rb^+	5.3	57.3	228	0.91	0.33
Cs^+	3.33	100	240	0.8	0.5
H^+‡	15	350	70	25	0.5

*Pooled data from differing anions.
‡HNO_3

3B4S″) and are formally identical for the four-site cases (Hägglund et al., 1978). From the satisfactory agreement between the theoretical curves and the experimental points it should be apparent that not only is the 1B4S′ model quite satisfactory in describing these data, but that the "foot" suggests the presence of an additional site. Note that the 1B4S′ model cannot give rise to the signs of "single filing" revealed by Lev's unidirectional flux ratio experiment, which requires the presence of additional rate-determining barriers near the channel mouth. Models with such barriers (e.g. a 3B2S′ model) can produce the proper flux ratio exponent of 2, or the conductance-concentration behavior, but not both (Hägglund et al., 1978). Models with more sites having the complexity of 3B4S′ or 3B4S″ are required to produce both behaviors in the proper concentration range.

Another conclusion from the present data is that there is no anion dependence of the shape of the G vs. G/a curves for representative alkali cations (K^+, Na^+, and Li^+) for which different anions (Cl^-, F^-, NO_3^-, and Ac^-) were tested. This finding is consistent with the membrane potential data to be presented below and with the prevalent view that there are no significant anion effects when studying group Ia cations.[3]

Thallous Salts

In contrast to the above situation for the alkali cations, where the 1B4S′ model was completely adequate, we found, while searching for more soluble Tl salts, an unex-

[3] It may be an oversimplification to consider anion binding to be negligible for the group Ia cations, in view of the evidence for its occurrence to be given in the case of Tl^+. Small but systematic differences among anions are visible in the data of Fig. 3. For example, the conductances of K, Na, and Li, although similar for different anions at the highest concentrations (for the reasons to be described for Tl^+ salts), are consistently higher at medium and low concentrations for the nitrates than for the other anions, and this difference is too large to result from uncertainties as to the legitimacy of assuming the activity coefficients of the cations to be equal to the mean activity coefficients of the salts. Since these differences do not alter the *shape* of the G vs. G/a relationship sufficiently to require extensions of the model in the way we will find necessary for Tl^+, we will neglect them here. However, this insensitivity of shape may turn out to be a consequence of the close spacing of first and second binding constants for those group Ia cations so far examined (K^h differs from K^0 by about a factor of 200 for Tl^+ but by less than a factor of 60 for K^+, Na^+, and Li^+).

pected effect of different anions. Although this effect is small, it is not negligible and is illustrated in the four separate plots for TlCl, TlAc, TlF, and $TlNO_3$ presented in Fig. 4. In these plots the experimental values of single channel conductances of valine gramicidin A in GMO/hexadecane bilayers are plotted as points and compared with solid theoretical curves drawn according to the extended model (Eq. 2) by using the parameters of Table II and the indicated values of anion binding constants (in M^{-1}). For comparison, the dashed curves labeled "0" give the expectations in the absence of anion binding that are the same as those for our original model (Eq. 3). The most striking feature of these data is the extremely vertical (actually z-shaped) G vs. G/a characteristic seen for $TlNO_3$. (An even more dramatic z-shape is also present in preliminary data obtained for $TlClO_4$ (Sandblom, Eisenman, and Neher, unpublished)). Such a z-shaped behavior, which implies a greater than first-power dependence of conductance on activity, is not explained by our original model, but can be understood as a consequence of postulating that anions can bind to the mouth of a Tl^+-occupied channel (which of course, has a positive charge), which is how we will extend our model in the section on Theory and Interpretation. The extremely steep slope seen at intermediate concentrations for TlF is also noteworthy and not reconcilable with our original model for any physically reasonable value of maximum limiting Tl^+ conductance, much less a value that is self-consistent with the data for Ac^- or Cl^-. The details of the curve fitting procedure used in constructing Fig. 4 will be deferred

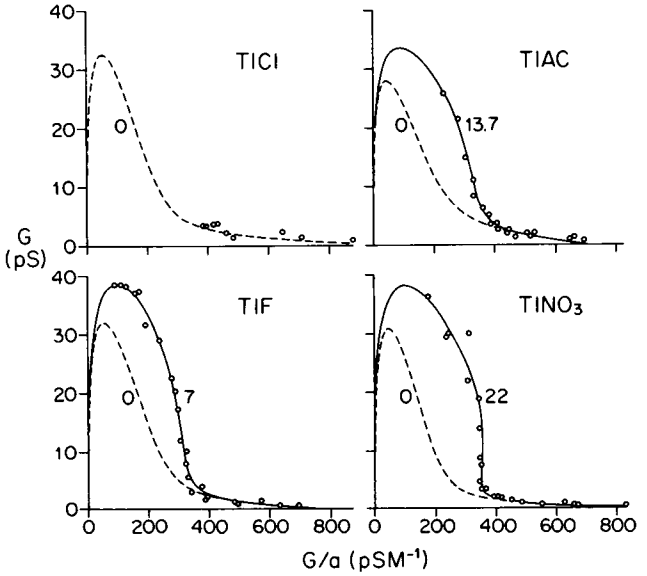

FIGURE 4 G vs. G/a (Eadie-Hofstee-type) plot for the single channel conductances of the indicated Tl^+ salts. Experimental data are plotted as points and compared with theoretical expectations given by the curves of the extended Eq. 2 in the case of zero anion binding (dashed curves labeled "0") and for the indicated values of anion binding (solid curves with values of $K_{a(Tl)}$ in M^{-1}). The parameters used to draw the theoretical curves are given in Table II.

TABLE II

"EXPERIMENTAL" PARAMETERS FOR FITTING Tl CONDUCTANCE DATA IN SYMMETRICAL SINGLE SALT SOLUTIONS ACCORDING TO THE MODEL "EXTENDED" FOR ANION BINDING EFFECTS

	$K_{a(x)}$	G_x^h	K_x^h	G_x^0	K_x^0	APS	AWS	K_x^∞
TlCl	0*	54.3*	4.72*	1.177*	759.9*	—	—	—
TlF	7	54.3	4.72	1.177	759.9	2	2	0.58
TlAc	13.7	46.6	4.61	2.247	315.3	2	2	0.60
$TlNO_3$	22	52.3	4.18	0.905	949.6	2	2	0.54
"Best"	0–50‡	54	4.7	0.8	1100	2	2	0.57

*For comparison the parameters for the theoretical curve for Cl^- were assigned the same as the for F^- but $K_{a(x)}$ was taken to be zero. The units of G's are pS and of K's M^{-1}.

‡This depends on the anionic species. 50 M^{-1} is the upper limit seen for the present anions in the potential data of Figs. 8 and 10.

to a later section, the present point being that such behavior of the G vs. G/a relationship is not possible for our original model. It is, however, understandable if one postulates the occurrence of anion binding to the outer sites of channels that have already bound a Tl^+ ion (Levitt, 1978, has suggested that such anion binding is necessary for the three-ion occupancy state of Tl^+ to be energetically reasonable.)

That different values of anion binding constants alone can produce these various G vs. G/a characteristics is apparent from the theoretical curves. How this happens physically can be grasped intuitively by considering the Eadie-Hofstee-type diagram in Fig. 5, which extends the two-site case of the right-hand side of Fig. 1 to include the possibility of also binding a nonpermeant anion (for simplicity, blocking effects are ignored). Consider the situation at low concentrations (to the right) first. Let us assume that the affinity of anions and cations for the channel is such that the anion can only bind significantly after a cation has been bound. From this we expect the x-intercept at low ion concentration ($G^0 \cdot K^0$) to be independent of the anion and we also expect to approach this intercept along the same asymptote (with slope = $1/K_x^0$) as in the previous two site case. Now consider the situation in the high concentration limit. Here, if there is no anion binding we have the same expectations as before, namely a curve asymptotic to the dashed line of slope = $1/K_x^h$. However, if anion binding begins to occur at concentrations between the binding of the first cation and the second cation, this would be expected (electrostatically) to increase the binding constant for the second cation from its intrinsic value (K_x^h) in the absence of anion binding to a higher value(K_{xa}^h). This, of course, would decrease the slope of the high concentration asymptote to that indicated by the solid line of slope = $1/K_{xa}^h$. Finally, in the simple situation diagrammed here, where binding an anion shifts the wells and peaks for cation permeation equally (which will be shown below to be in accord with the data), we expect the y-intercept at high concentrations (G_{xa}^h) to be independent of anion binding, because the barrier height (being the peak-well difference) is unaltered by anion binding. If the shift of well and peak are not exactly the same, there

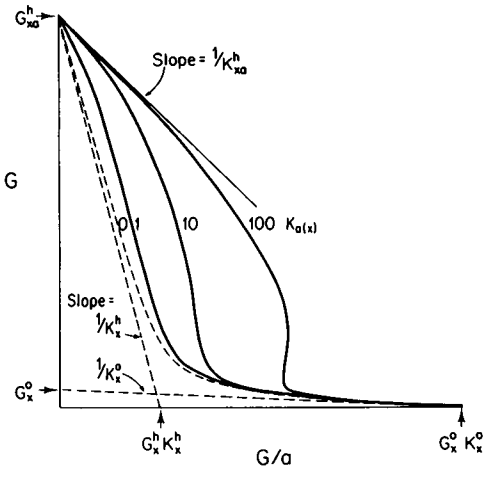

FIGURE 5

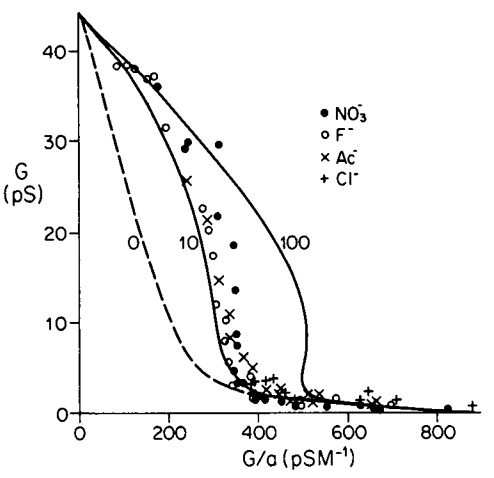

FIGURE 6

FIGURE 5 Schematic representation of the effects of anion binding, expected from the extended Eq. 2, on the G vs. G/a (Eadie-Hofstee-type) plot. For simplicity, peak and well shifts have been assumed equal and blocking effects have been omitted. Notice that in the low concentration limit all curves have the same asymptote, whose slope is $1/K^0_x$. The high concentration curves in the absence of anion binding ($K_{a(x)} = 0$) are asymptotic to the line of slope $1/K^h_x$; whereas when there is anion binding the curves become asymptotic to the line of slope $1/K^h_{xa}$. Notice that the y-intercept at high concentrations is the same in the absence as in the presence of anion binding ($G^h_x = G^h_{xa}$).

FIGURE 6 G vs G/a (Eadie-Hofstee-type) representation of single-channel conductance data for the indicated Tl^+ salts, indicating the similarity of conductances at highest concentrations. Notice that the vertical differences seen for different anionic salts at given values of G/a become negligible both at high and low concentrations. The data can be compared with theoretical expectations of the extended Eq. 2 (neglecting blocking effects) for zero anion binding (curve "0") as well as for anionic binding constants ($K_{a(Tl)}$) of 10 and 100 M^{-1}.

should be shifts in the y-intercept, which in principle could be seen by comparing a nonbinding anion with a strongly binding one. In practice, not having a soluble salt of Tl^+ with a nonbinding anion, we can only compare anions having different degrees of binding.

To recapitulate, binding an anion is expected (electrostatically) to lower the potential energy profile for cation permeation, thereby increasing the binding constant for the high concentration region from its value in the absence of binding (K^h_x) to a new, and higher, value (K^h_{xa}). If it also lowers the wells and peaks to an approximately equal extent, there will be no change in the barrier height, leaving the y-intercept unaltered ($G^h_{xa} = G^h_x$).

In the light of the above discussion of Fig. 5, one of the most important aspects of the conductance data for various Tl^+ salts is the finding that the conductances at high concentrations do, indeed, become independent of the anion. This finding also indicates that anion conductances at these concentrations are negligible, which agrees with independent estimates from membrane potentials which indicate that anion conduc-

tance never exceeds 10% of Tl^+ conductance (Eisenman, Sandblom and Neher, unpublished observations). That the conductances at high concentrations are independent of the anion is best seen by plotting the Tl^+ data for the four different anions on a common figure, as in Fig. 6, which for reference also presents certain theoretical curves from Fig. 5. The solid curves correspond to the extended model (Eq. 2), neglecting block, for the indicated values of anion binding constant. Notice that the data for all the anions studied fall nicely into a region corresponding to a binding constant between 10 and 100 M^{-1}. But, most importantly, notice the similarity of the conductances seen for the different anions in the high concentration range (at the left). This finding, together with the above described inference that anion binding shifts the cation wells downward, implies that wells and peaks are shifted equally by anion binding. Moreover, analysis of the data of Fig. 3 and Table II for each anion separately will further support this conclusion (see later discussion of Table II). All theoretical curves in Figs. 3–6 have been drawn assuming not only that the well and peak are shifted equally for a given anion, but also to the same extent for all anions (anion peak shift [APS] = anion well shift [AWS] = 2, defined in Eqs. 4 and 5).

We should also point out that the results at the lowest concentrations are also consistent with the expectations of both the extended model and the original model. In particular, the "foot" at low concentrations due to the postulated high-affinity Tl^+ binding site is seen to be present for all anions. It can also be seen that the Tl^+ conductances become independent of the anion at the lowest concentrations, as they should theoretically, and—of particular importance for comparison with the membrane potential data—that the x-intercepts (seen most clearly in Fig. 4 and Table II) are also virtually independent of the anion. Note that only at intermediate concentrations are significant differences in conductance expected theoretically. This is because there should be no anion binding at low concentrations, and no differences at the highest concentration if peaks and wells are shifted equally.

Even if one chooses to ignore the above detailed interpretations, the conclusion is inescapable that the value of the high conductance intercept, G^h, estimated from data with F^-, NO_3^-, and Ac^- salts with the aid of the extended model, would be independent of the anion and provides a more accurate estimate of G^h, and consequently of K^h and K^∞, than was possible from the limited data presented previously for Cl^- (owing to poor solubility), for which no anion effects were detected.

MANY-CHANNEL MEMBRANE POTENTIALS

This section will now characterize the ion concentration dependence of the permeability ratio, P_{Tl}/P_K, measured with the Goldman-Hodgkin-Katz equation from membrane potentials at zero current in Tl^+-K^+ mixtures. A wider concentration range, using F^-, NO_3^-, and Ac^- salts, is characterized than was permitted by solubility limitations in our previous work on Cl^- salts. To elucidate further possible specific effects of anions, some limited results for a number of other anionic species will also be described.

Because the precise form of the concentration dependence of P_{Tl}/P_K is likely to be critical in distinguishing between the present 1B4S′ model and alternative models, the concentration dependence must be characterized carefully; and a few comments on experimental design and precautions are appropriate. First, no conventional salt bridge is adequate for measuring the membrane potentials, as precipitation can occur in the junction because of the limited solubility of Tl^+ salts with the usual bridge electrolytes (KCl, NH_4NO_3). Our usual chlorided silver electrodes (cf. Szabo et al., 1969) have proven satisfactory, but certain precautions are necessary. For example, when Cl^- was not the principal anion, 10^{-4}M was added as a "trace" component; and as a control for "poisoning" of AgCl electrodes by Tl^+ at high concentrations, we routinely measured the potential under symmetrical conditions both before and after all measurements of membrane potential. This enabled any drift in the AgCl electrodes to be canceled out. Such drifts are quite small in the usual experiments, where mixtures of cations are formed by additions to initially symmetrical single salt solutions (cf. V^{obs} in Table V of Eisenman et al., 1977). However, conventional "bi-ionic" measurements (e.g. Myers and Haydon, 1972) are unreliable for Tl^+ since residual asymmetry potential differences observed on making the solutions symmetrical after the bi-ionic measurement are surprisingly large. Since all the information of the bi-ionic measurements (and more) can be obtained by going to the appropriate limits of salt mixtures, we have avoided the bi-ionic situation in this work. In addition, it is unwise to rely on bi-ionic measurements solely, because important distinguishing characteristics of the various models appear in their different expectations for two-sided vs. one-sided variations of the ion concentration.

As a further control on electrode artifacts and on the adequacy of the activity coefficient assumptions necessary to interpret the data, we performed duplicates of critical experiments with nonactin. We used the fact that the value of P_{Tl}/P_K for nonactin is sufficiently close to the average value for gramicidin that controls could be run under identical solution conditions (Eisenman, Sandblom, and Neher, to be published). Lastly, since we have previously established (Eisenman et al., 1977, Fig. 9) that single channel permeability ratios agree with those for a macroscopically conducting (many-channel) membrane, we rely here on data obtained using the easier and more precise many-channel measurements. Most of the data are taken in situations in which anion permeability can be assumed to be negligible. However, in the limit of high (symmetrical) concentrations of Tl^+, experiments of the type of Fig. 18 and Table V of Eisenman et al. (1977) indicate that anion permeation cannot be neglected (except in the case of $SO_4^=$) and we correct for it by a semi-empirical method to be described in the text. Sufficient gramicidin was added from ethanolic stock solutions to produce a membrane conductance between 100 and 10,000 times greater than that of the naked bilayer (even after increasing the salt concentration) to avoid concentration polarization.

Figs. 7 and 8 summarize the permeability ratios measured as described elsewhere (Eisenman et al, 1977) in Tl^+-K^+ mixtures in the presence of various anions under the conditions indicated schematically in the insets of each subfigure. Fig. 7 presents

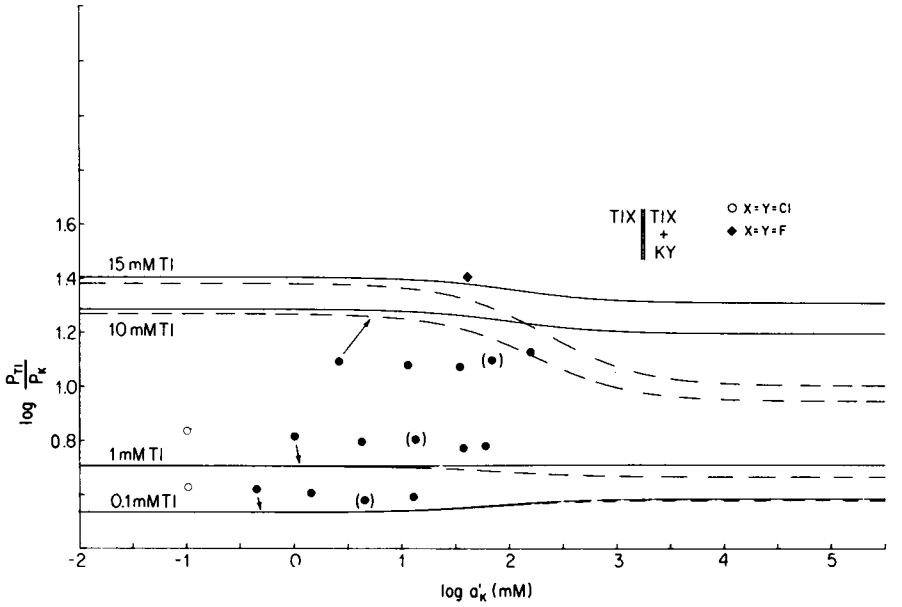

FIGURE 7 Experimentally observed data points and theoretically calculated curves from the concentration dependence of P_{Tl}/P_K for four different bilateral concentrations of thallium as a function of varying the one-sided K^+ concentration. The inset indicates the experimental conditions (valine gramicidin A, GMO/decane bilayers for all many-channel membrane potential data). The theoretical curves are drawn from the extended Eq. 14 for the values of parameters in Table IV with an anion binding constant of 10 M^{-1} solid curves and 0 (dashed curves). The data at 15 mM Tl^+ were obtained with fluoride as the sole anion (except for a 10^{-4} M trace of Cl^-); whereas the data in the lower three curves were obtained with pure chlorides (open circles) with increasing (one-sided) concentrations of nitrate. The theoretical curves are drawn for the ionic activities of the initially symmetrical salts, but neglect further (one-sided) changes in these activities with increasing ionic strength due to addition of the K^+ salt. The parenthesized data points (at approximately 10:1 ratio of K^+ to Tl^+) will be included in Fig. 10 for comparison with the data at bilaterally symmetrical 10:1 K^+:Tl^+ ratio. Notice that the permeability ratios in this figure are measured in a gradient of K, whereas those in Fig. 8 are measured in a gradient of Tl. If there is any anion permeation, the measurements in a gradient of Tl underestimate the true values whereas those in a gradient of K overestimate it. Anion permeability should be negligible for the measurements below 10 mM Tl in this figure (and for all of the measurements in Fig. 8). For the 15 mM symmetrical TlF data point the "true" value of the $P_{Tl}/P_K = 26$, corrected for F^- permeation, has been estimated as the geometric mean of the "apparent" values measured in a gradient of thallium and a gradient of potassium. Arrows indicate the curves corresponding to the experimental data points. •, X = Cl; Y = NO_3.

the data for symmetrical thallium salts under the conditions of one-sided addition of the indicated potassium salts, while Fig. 8 presents the data for symmetrical potassium salts with one-sided additions of the indicated thallium salts. The points represent experimentally measured permeability ratios calculated from the potential measurements with the Goldman-Hodgkin-Katz-type membrane potential equation (Eisenman et al., 1977, Eq. 1). We assume negligible anion permeability and use a Brönsted-Kielland-type activity coefficient correction. These data points can be compared with theoretical

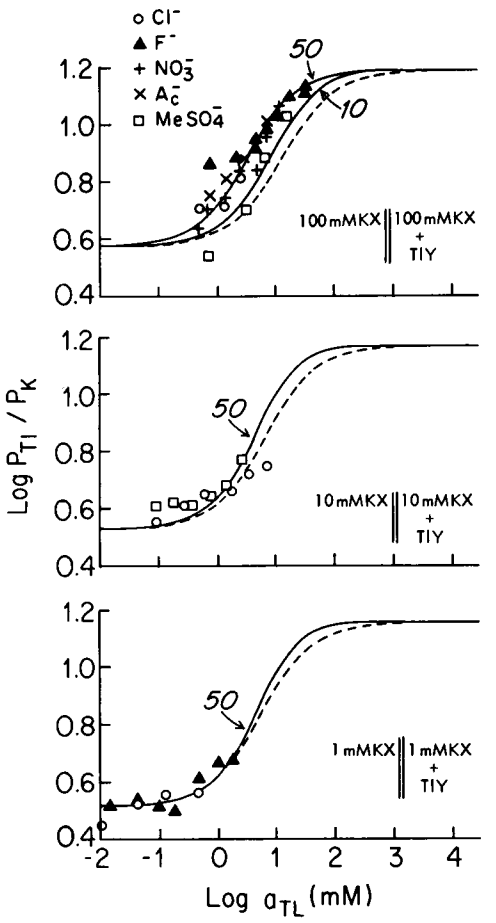

FIGURE 8

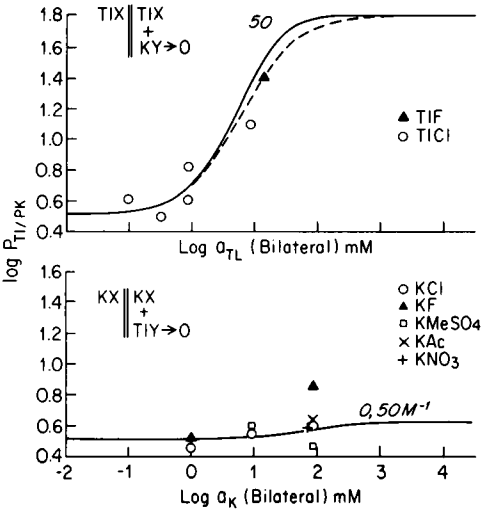

FIGURE 9

FIGURE 8 Experimentally observed data points and theoretically calculated curves showing the dependence of the permeability ratio (P_{Tl}/P_K) on ionic activities in systems in which potassium is varied symmetrically bilaterally and Tl^+ is varied on one side. The dashed curves correspond to zero anion binding, the solid curves have been drawn for the indicated anion binding constants in M^{-1}. Activity coefficients for the individual ions in Figs. 7 and 8 have been calculated with a Brönsted-Kielland-type approximation in which the activity coefficients of Tl^+ and K^+ have been assumed to equal the mean activity coefficients in their pure Tl^+ salts at the ionic strength of the solution, and in which the activity coefficient for Cl^- was assumed to be that of the mean activity coefficient of the chloride salt of the predominant cation at the ionic strength of the mixture (or of an appropriate average). The anion species X^- is identified by the symbols; the species Y^- was NO_3^- except in the case of F^- where both X^- and Y^- were F^-.

FIGURE 9 Dependence of P_{Tl}/P_K on symmetrical Tl^+ concentration (upper) and symmetrical K^+ concentration (lower). Experimental data points come from the left-hand limits of Figs. 7 and 8 (extrapolating where necessary). In the upper figure the dashed theoretical curve is for zero anion binding, and the solid theoretical curve for an anion binding constant of 50 M^{-1}. In the lower figure a single theoretical curve is expected under the approximation (Eq. 16) that anions do not bind to K^+ loaded channels but only to Tl^+-loaded ones. That this approximation is not adequate above 100 mM is suggested by the spread of data for the different (one-sided) anions at the right of the lower figure. The highest concentration data for F^- here and in Fig. 8 suggest that there may actually be binding of F^- to channels loaded with cations other than Tl^+.

curves calculated according to the extended theory (Eqs. 14 and 15, solid curves) for the indicated anion binding constants (10 M^{-1} in Fig. 7 and 10 M^{-1} and 50 M^{-1} in Fig. 8). The expectations of our original theory corresponding to zero anion binding (Eq. 13) are given by the dashed curves in all figures. Fig. 9 summarizes the dependence of P_{Tl}/P_K on the bilateral Tl^+ (upper) and bilateral K^+ (lower) activities in the important limits of zero K^+ and Tl^+ concentrations, respectively, obtained from the low concentration limits (at the left) of Figs. 7 and 8. Considering that the parameters are chosen to describe the data of Fig. 10 also, it should be clear that the theoretical curves adequately describe the experimental data and that anion binding effects are only observed at the highest concentrations, above 100 mM. Indeed, anion effects are not striking in the permeability data; nor are they expected to be from the theory because in the present electrostatic approximation anion binding changes no limits but merely shifts the concentrations at which the changes in P_{Tl}/P_K occur.

Although the measurements of Figs. 7–9 suffice to assess the theoretical parameters, a more extended measurement of the parameters, as well as a further test of the

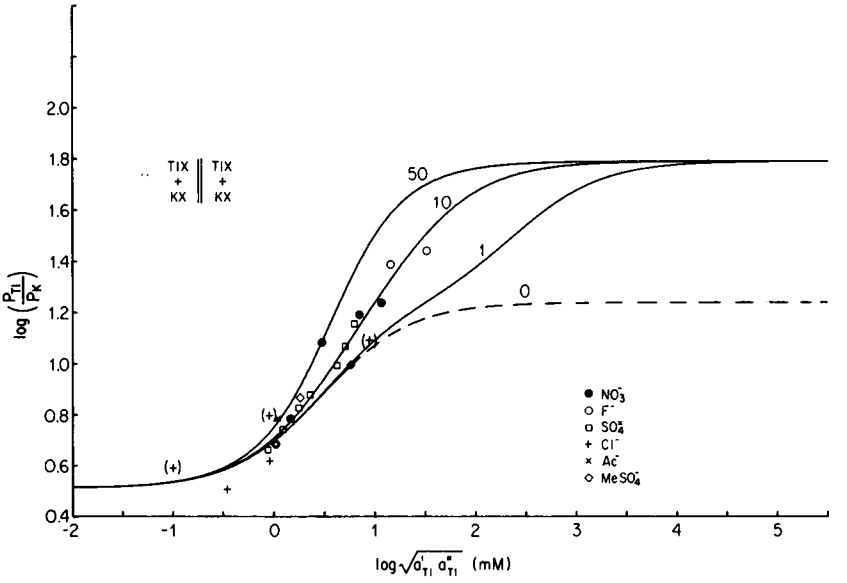

FIGURE 10 Dependence of P_{Tl}/P_K on the geometric mean of the Tl^+ activities on both sides of the membrane in experiments in which Tl^+ and K^+ are varied bilaterally for the indicated anions. Only "true" values of permeability ratio have been plotted, estimated as the geometric mean between those measured in a gradient of K^+ and in a gradient of Tl^+. Since the experiments were carried out under conditions in which the potassium concentration was always about 10 times the thallium concentration, the experimental points are compared with the theoretically expected trajectories calculated for a K^+ activity 10 times larger than the Tl^+ activity. The dashed curve is for zero anion binding, the solid curves for $K_{a(Tl)}$ = 50, 10, and 1 M^{-1}. For completeness, three additional (parenthesized) data points are included for Cl^-. These are the points from the experiments of Fig. 7 at 10:1 K^+:Tl^+ ratio on one side only, with K^+ on the other side being zero. If Cl^- binding is really zero, the absence of K^+ on one side is not expected to affect the position of these points.

theory, and an assessment of the magnitude of possible anion permeability effects, are possible under the experimental conditions of Fig. 10, where both K^+ and Tl^+ are simultaneously varied bilaterally. This figure represents the pooled results of experiments in which the concentration of both K^+ and Tl^+ were incrementally increased and permeability ratios were successively measured in the presence of small gradients of either species. One set of points was obtained for each anion NO_3^-, F^-, $MeSO_4^-$, Ac^-, and $SO_4^=$ in individual experiments, while the two unparenthesized data points for Cl^- came from separate experiments. Experimental values for the "true" permeability ratios are plotted as points. These have been estimated as the geometric mean of the "apparent" permeability ratios measured in a gradient of K^+ and in a gradient of Tl^+. This circumvents any errors introduced by possible anion permeation at high bilateral Tl^+ concentration, as will be discussed below. Although detailed differences among anions are not obvious in Fig. 10, the data for Cl^- and $MeSO_4^-$ both lie suggestively close to the theoretical curve for zero anion binding; whereas the F^- and NO_3^- data are more in accord with a significant degree of anion binding, consistent with the other conductance and potential measurements of this paper.

Anion Permeability Effects

Relative to Tl^+, anion permeability is always negligible, as indicated by the conductance studies and confirmed by potential measurements to be described below. Unfortunately, at very high symmetrical Tl^+ concentrations it is not always negligible in relation to K^+, which complicates the interpretation of the potential data under these conditions. Depending on the external solution conditions, the "apparent" permeability ratio will then be either an overestimate or an underestimate of the true permeability ratio (for details see Table V and Fig. 18 of Eisenman et al., 1977). Fortunately, the effects of anion permeation can be approximately corrected for by taking the geometric mean of the "apparent" permeability ratio measured in a gradient of Tl^+ vs. that measured in a gradient of K^+ for the same symmetrical initial conditions (Eisenman, Sandblom, and Neher. To be published). Experiments carried out under such conditions, together with appropriate nonactin controls that activity coefficient corrections have been properly made, indicate that $SO_4^=$ is virtually impermeant over most of the experimental range and that the "true" permeability ratios corrected for a small anion permeability of the other anions are internally consistent with those measured for $SO_4^=$ (recall Fig. 10).

THEORY AND INTERPRETATION

The above described results can be interpreted quantitatively by extending our previous 1B4S' model (Sandblom et al., 1977) to include the effects of anion binding (Sandblom, Eisenman, and Neher. To be published). Despite Lev's new observations on single-filing, which make it no longer reasonable to assume the cation sites to be in equilibrium with the solution, the anions are assumed to bind only to sites assumed to be in equilibrium with the external solution. It seems likely that such an "equilibrium

theory" for anion effects on cation permeation will be capable of appropriate "translation" to the model that ultimately proves to be best for cation permeation, presently viewed as a phenomenological "black box" in terms of the "experimental" parameters.

To extend our previous model we need only to assume that binding of an anion species, A^-, can occur to a cation-loaded outer site, thus forming two additional states,

$$X_oA \quad \text{and} \quad X_oX_iA \tag{1}$$

for each half channel. These states correspond to the loading of an anion species A^- in the presence of cation species X^+ bound to the outer site (state X_oA) and to both the outer and inner sites (state X_oX_iA) in each half of the symmetrical gramicidin channel. The new states differ from those in the absence of anion binding by appropriate shifts in the levels of the various energy wells and peaks which a cation encounters in passing through the channel. (Recall Fig. 13 of Eisenman et al., 1977, and Fig. 4 of Sandblom et al., 1977, for examples of corresponding energy shifts produced cation-binding).

Single Channel Conductance

These two new half-channel states contribute additional terms to our previous expression for N_s, the fraction of time the channel is completely empty; and this causes the expression for single channel conductance to become extended from its previous form by the inclusion of two new terms dependent on anion binding, $(1 + 0.5K_{a(x)} \cdot C_a\sqrt{\text{APS}})$ and $(1 + 0.5K_{a(x)}C_a\sqrt{\text{AWS}})$, which introduce the effects of the anion binding constant $K_{a(x)}$) and of the concentration of anions (C_a) as well as of the APS and the AWS. For a single salt, of course, $C_a = C_x$. (Please note that the dimensionless parameters APS and AWS are called "shifts" because kT times the log of their values corresponds to shifts in the energy profile on plots like Figs. 1 or 13).

The extended equation becomes:

$$G_x(A) = \frac{G_x^0K_x^0[1 + 0.5K_x^0C_x(1 + 0.5K_{a(x)}C_a\sqrt{\text{APS}})(G_x^hK_x^h/G_x^0K_x^0)^{1/2}]^2C_x}{[1 + 0.5K_x^0C_x(1 + 0.5K_{a(x)}C_a)]^2 + K_x^hC_x[0.5K_x^0C_x(1 + 0.5K_{a(x)}C_a\sqrt{\text{AWS}})]^2(1 + K_x^\infty C_x)} \tag{2}$$

which, of course, reduces to our previous one in the absence of anion-binding.

$$G_x = \frac{G_x^0K_x^0[1 + 0.5K_x^0C_x(G_x^hK_x^h/G_x^0K_x^0)^{1/2}]^2C_x}{[1 + 0.5K_x^0C_x]^2 + K_x^hC_x[0.5K_x^0C_x]^2(1 + K_x^\infty C_x)}. \tag{3}$$

There are three additional parameters ($K_{a(x)}$, K_{xa}^h, and G_{xa}^h) in the extended conductance expression (no additional anion parameter is introduced if it is assumed that AWS is unaltered by loading the opposite inner site). The values of K_{xa}^h and G_{xa}^h which determine the "peak shifts" and "well shifts" produced by anions through:

$$G_{xa}^hK_{xa}^h/G_x^hK_x^h = \text{APS}, \tag{4}$$

$$K_{xa}^h/K_x^h = \text{AWS}, \tag{5}$$

TABLE III

"TRANSLATION" BETWEEN "EXPERIMENTAL" PARAMETERS AND PHYSICAL PARAMETERS FOR THE 1B4S' MODEL

"Experimental" parameter	How measured	Physical parameters
	Permeability ratios, P_x/P_y, from zero-current potentials in ionic mixtures	
Original model		
$\alpha = \frac{\alpha_x}{\alpha_y}$	$\alpha = \frac{P_x}{P_y}$ when $c_x \to 0, c_y \to 0$	$\frac{v_{x_i} \cdot k_{x_i}}{v_{y_i} \cdot k_{y_i}}$
β_x, γ_x	$\alpha\left(\frac{\beta_x}{\gamma_y}\right)^2 = \frac{P_x}{P_y}$ when $c_x \to \infty, c_y \to 0$	$k_{x_o}\left[\frac{v_{x_i}^{x_o x_o} \cdot k_{x_i}^{x_o x_o}}{v_{x_i} \cdot k_{x_i}}\right]^{1/2}$, $k_{x_o}\left[\frac{v_{y_i}^{x_o x_o} \cdot k_{y_i}^{x_o x_o}}{v_{y_i} \cdot k_{y_i}}\right]^{1/2}$
β_y, γ_y	$\alpha\left(\frac{\beta_y}{\gamma_y}\right)^2 = \frac{P_x}{P_y}$ when $c_y \to \infty, c_x \to 0$	$k_{y_o}\left[\frac{v_{x_i}^{y_o y_o} \cdot k_{x_i}^{y_o y_o}}{v_{x_i} \cdot k_{x_i}}\right]^{1/2}$, $k_{y_o}\left[\frac{v_{y_i}^{y_o y_o} \cdot k_{y_i}^{y_o y_o}}{v_{y_i} \cdot k_{y_i}}\right]^{1/2}$
Extended for anions		
θ_{xa}, ϕ_{xa}	$\alpha\left(\frac{\beta_x}{\gamma_y}\frac{\theta_{x_i}}{\phi_{x_i}}\right)^2 = \frac{P_x}{P_y}$ when $c_x \to \infty, c_y \to 0$	$k_a^{x_o}\left[\frac{v_{x_i}^{x_o x_o aa} \cdot k_{x_i}^{x_o x_o aa}}{v_{x_i}^{x_o x_o} k_{x_i}^{x_o x_o}}\right]^{1/2}$, $k_a^{x_o}\left[\frac{v_{y_i}^{x_o x_o aa} \cdot k_{y_i}^{x_o x_o aa}}{v_{y_i}^{x_o x_o} k_{y_i}^{x_o x_o}}\right]^{1/2}$
θ_{ya}, ϕ_{ya}	$\alpha\left(\frac{\beta_y}{\gamma_y}\frac{\theta_{ya}}{\phi_{ya}}\right) = \frac{P_x}{P_y}$ when $c_y \to \infty, c_x \to 0$	$k_a^{y_o}\left[\frac{v_{x_i}^{y_o y_o aa} \cdot k_{x_i}^{y_o y_o aa}}{v_{x_i}^{y_o y_o} k_{x_i}^{y_o y_o}}\right]^{1/2}$, $k_a^{y_o}\left[\frac{v_{y_i}^{y_o y_o aa} \cdot k_{y_i}^{y_o y_o aa}}{v_{y_i}^{y_o y_o} k_{y_i}^{y_o y_o}}\right]^{1/2}$

are measurable from plots of G vs. G/a through the limiting expression 6 in the absence of block:

$$G_x(A) = G_{xa}^h - (G_x/C_x)(1/K_{xa}^h), \tag{6}$$

and expression 7 in the presence of block

$$\log G_x(A) = \log G_{xa}^h \cdot (K_{xa}^h/K_x^h) - \log C_x K_x^\infty, \tag{7}$$

as has already been mentioned in relation to Figs. 4–6. These correspond to the previous expressions in the absence of anion binding:

$$G_x = G_x^h - (G_x/C_x)(1/K_x^h), \tag{8}$$

$$\log G_x = \log G_x^h - \log C_x K_x^\infty. \tag{9}$$

The blocking constant K_x^∞, is estimating by curve fitting the full Eq. 2.

TABLE III (*continued*)

"Experimental" parameter	How measured	Physical Parameters
	Individual channel conductances (in single salts)*	
Original model		
$G_x^0, G_y^0,$	y intercept of low concentration asymptote (Eq. 10)	$\frac{1}{2}v_{xi}\cdot(k_{x_i}/k_{x_o})$, $\frac{1}{2}v_{y_i}\cdot(k_{y_i}/k_{y_o})$
$G_x^h, G_y^h,$	y intercept of high concentration asymptote (Eq. 8)	$\frac{1}{2}v_{x_i}^{x_o x_o}$, $\frac{1}{2}v_{y_i}^{y_o y_o}$
$K_x^0, K_y^0,$	1/slope of low concentration asymptote (Eq. 10)	$2k_{x_o}$, $2k_{y_o}$
$K_x^h, K_y^h,$	1/slope of high concentration asymptote (Eq. 8)	$2k_{x_i}^{x_o x_o}$, $2k_{y_i}^{y_o y_o}$
K_x^∞, K_y^∞	Blocking behavior (Eq. 9)	$\frac{1}{2}k_{x_i}^{x_o x_o x_i}$, $\frac{1}{2}k_{y_i}^{y_o y_o y_i}$
Extended to anions		
$K_{a(x)}, K_{a(y)}$	Anion binding constant (Eq. 2)	$2k_a^{x_o}$, $2k_a^{y_o}$
G_{xa}^h, G_{ya}^h	y intercept of high concentration asymptote (Eq. 6)	$\frac{1}{2}v_{x_i}^{x_o x_o aa}$, $\frac{1}{2}v_{y_i}^{y_o y_o aa}$
K_{xa}^h, K_{ya}^h	1/slope of high concentration asymptote (Eq. 6)	$2k_{x_i}^{x_o x_o aa}$, $2k_{y_i}^{y_o y_o aa}$
K_x^∞, K_y^∞	Blocking behavior (Eq. 7)	$\frac{1}{2}k_{x_i}^{x_o x_o x_i aa}$, $\frac{1}{2}k_{y_i}^{y_o y_o y_i aa}$

*The "experimental" conductance parameters (in Siemens) should be multiplied by $2kT/e^2$ ($3.22 \times 10^{17}\ S^{-1} \times s^{-1}$ at 25°C) to obtain the physical rate constants in s^{-1}. To convert from the concentration units (liters per mole) in which the "experimental" binding constants are expressed to dimensionless mole fraction units more appropriate to the physical binding constants, the former should be multiplied by 55.5 mol H_2O/liter.

The low concentration limit is, of course, the same, and independent of anions, being

$$G_x = G_x^0 - (G_x/C_x)(1/K_x^0), \tag{10}$$

in the extended, as in the previous, treatment since anion binding has been assumed not to occur until after a cation is bound.

Comparison of Eqs. 4 and 5 (or of 6 and 8 or 7 and 9) leads to the conclusion that the conductance in the high concentration limit (the y-intercept on the Eadie-Hofstee-type plot) will be shifted from that in the absence of anion binding by the ratio

$$(G_x(A)/G_x)_{c_{xa}\to\infty} = G^h_{xa}/G^h_x, \tag{11}$$

which gives a measure of the shift in barrier height, relative to the well, on loading the anion, the "anionic barrier shift" (ABS = APS/AWS). This is defined not only in terms of the experimental parameters G^h_{xa} and G^h_x but also in terms of the physical parameters (rate constants) of our model (Table III).

$$\text{ABS} = G^h_{xa}/G^h_x = v^{x_o a x_o a}_{x_i}/v^{x_o x_o}_{x_i}. \tag{12}$$

That this barrier shift is small is indicated by the convergence of the higher concentration data for all anions seen in Fig. 6, as mentioned previously. This implies that the effect of anion binding is seen equally on the well and on the peak, as would be expected from a purely electrostatic effect if the edge of the barrier is near the well, as it would be for a trapezoidal barrier more realistic than the present oversimplified sharp one. To estimate the values of APS and AWS more precisely we carried out a least squares computer analysis for the TlF data in the region where block could be neglected (up to 0.5 M) to obtain the best fit (neglecting block) of the five parameters of Eq. 2 (G^0_{Tl}, K^0_{Tl}, $K_{a(x)}$, APS, AWS), which were allowed to vary freely, while fixing only the values of G^h_{Tl} and K^h_{Tl} (45 ps and 5 M^{-1}). Convergence was obtained; and the following values produced a very satisfactory visual fit to the data (G^0_{Tl} = 1.177 ± 0.16 pS; K^0_{Tl} = 750 ± 134 M^{-1}; $K_{F(Tl)}$ = 13.3 ± 0.44 M^{-1}; APS = 1.976 ± 0.006; AWS = 1.922 ± 0.009; ± SD).

The values of APS and AWS produced by F^- were both found to be sufficiently close to 2 that, since comparable values were also found with the data for $TlNO_3$ and only slightly higher values with the data for TlAc, it seemed reasonable to simplify things by assuming that the peak shift is not only the same as the well shift for a given anion, but that it also has the same value, about 2, for all anions (consistent with a purely electrostatic effect). With this approximation, only one free parameter, $K_{a(x)}$, the binding constant of the anion, remains to account for the effects of all the monovalent anions studied. The adequacy of the theory, so simplified, to describe the data for F^-, NO_3^-, Ac^-, and Cl^- can be seen in Fig. 4, where the curves were drawn using this assumption according to the parameters given in Table II.

Several details are worth noting about the parameters in Table II. First, is the close agreement between the values of G^h_x for TlF and $TlNO_3$ and the not greatly lower value for TlAc. Second, the assumption that all monovalent anions produce the same (electrostatic) effects on binding constants is borne out by the similar values calculated for the intrinsic high concentration binding constants for Tl^+ (K^h_x, K^∞_x), despite the differences in the curves for the various anions. Third, whether the apparent systematic differences in the individual values of the zero concentration limiting parameters (G^0_x, K^0_x) (which, however, still produce nearly the same x-intercept [$G^0_x \cdot K^0_x$], as demanded by theory), are real or artifactual cannot yet be resolved. The limiting values should be independent of the anion; and it is possible, indeed, to assign a common

value (G_x^0 = 0.8 pS, K_x^0 = 1,100) to all these species, which probably best represents reality, and is for that reason labeled "best" in Table II.

Having now presented the basis for our interpretations of the much more extensive data on single channel conductances for Tl^+ obtainable with the more soluble TlF, TlAc, and $TlNO_3$ salts than was possible previously for TlCl, we may now comment on certain important features of the conductance-concentration behavior.

First is the existence of a maximum in conductance at high concentrations of Tl^+, not previously seen but expected both from the model and by analogy to the maximum seen with the group Ia cations. This is most convincingly shown in the data for TlF in Fig. 4, but the effect is also present for $TlNO_3$ and TlAc, as indicated in Fig. 4 by the convexity of their curves at high concentrations. The effect is measurable in terms of the theory by the value of the parameter K_x^∞ extracted from least squares best fits to the data according to Eq. 2 (notice the very similar values of K_x^∞ for F^-, AC^-, and NO_3^- in Table II). Interestingly, the value of K_x^∞ for Tl^+ will be seen in Fig. 11 to follow the same trends relative to K_x^h and K_x^0 observed for the comparably sized group Ia cations.

Second, the new and more extensive data for TlCl presented here in Fig. 4, obtained for freshly formed membranes (see Neher et al., 1978), are quite comparable to those previously reported (Eisenman et al., 1977; Sandblom et al., 1977) for the usual aged membranes. However, the data for the other anions now enable us to revise our estimate for G^h for Cl (since this should be the same for all anions) to 54.3 pS (see Table II), much higher than that of 10.4 pS we previously made from the very limited range of data available for TlCl, owing to its insolubility above 10 mM. The reasons for this should be apparent from the theoretical curve (for zero anion binding) given in Fig. 4 for comparison with the TlCl data. Clearly the expected major curvature occurs at concentrations too high to be reliably measured in TlCl. It is indeed somewhat surprising that we were even able to detect the relatively small curvature of the tail in our original experiments.

Membrane-Potentials at Zero Current

The effects of anion-binding also contribute additional terms to our previous expressions for the permeability of X and Y, as measured by the zero current membrane potentials in cationic mixtures. The β and γ parameters of our previous expression,

$$P_x/P_y = \alpha[(1 + \beta_x c_x' + \beta_y c_y')(1 + \beta_x c_x'' + \beta_y c_y'')]/ [(1 + \gamma_x c_x' + \gamma_y c_y')(1 + \gamma_x c_x'' + \gamma_y c_y'')] \quad (13)$$

now become dependent on the anion concentration, as defined by the extended expression

$$P_x/P_y = \alpha[(1 + \beta'_{xa} c_x' + \beta'_{ya} c_y')(1 + \beta''_{xa} c_x'' + \beta''_{ya} c_y'')]/ [(1 + \gamma'_{xa} c_x' + \gamma'_{ya} c_y')(1 + \gamma''_{xa} c_x'' + \gamma''_{ya} c_y'')], \quad (14)$$

where the β's and γ's now depend on the anion concentrations

$$\begin{aligned}
\beta'_{xa} &= \beta_x(1 + \theta_{xa}c'_a), \quad \beta''_{xa} = \beta_x(1 + \theta_{xa}c''_a),\\
\beta'_{ya} &= \beta_y(1 + \theta_{ya}c'_a), \quad \beta''_{ya} = \beta_y(1 + \theta_{ya}c''_a),\\
\gamma'_{xa} &= \gamma_x(1 + \phi_{xa}c'_a), \quad \gamma''_{xa} = \gamma_x(1 + \phi_{xa}c''_a),\\
\gamma'_{ya} &= \gamma_y(1 + \phi_{ya}c'_a), \quad \gamma''_{ya} = \gamma_y(1 + \phi_{ya}c''_a),
\end{aligned} \tag{15}$$

in which primes and double primes designate the appropriate anion concentrations. (For the usual experimental situation where mixtures of two monovalent cations and a common anion are studied, Eq. 15 can be expressed solely in terms of cation concentrations by the relationships $c'_a = c'_x + c'_y$; $c''_a = c''_x + c''_y$).

Although Eq. 15 introduces the possibility of four additional experimental parameters ($\theta_{xa}, \theta_{ya}, \phi_{xa}, \phi_{ya}$, defined in Table III) for the effects of anions,[4] we find it possible to make some simplifying assumptions and to represent the present data with only one additional experimental parameter, which physically corresponds to the product of the peak shift produced by the anion and the binding constant of the anion to the Tl^+-loaded channel.

The reasoning permitting this simplification is as follows: First, if we conclude from the conductance data of Fig. 3 that there is no significant anion binding to K^+-loaded channels we may assume that $k_a^{y_o} = 0$, recalling the definitions of Table III and identifying K^+ with Y and Tl^+ and X. In this way we can eliminate θ_{ya} and ϕ_{ya}, which both become zero when $k_a^{y_o} = 0$:

$$0 = \theta_{ya} = \phi_{ya}. \tag{16}$$

Such an assumption would imply that anion binding in the case of Tl^+ involves specific interactions. Probably, reality would be better represented by allowing for a finite anion binding constant to K^+-loaded channels, smaller than that for Tl^+; but present data are not sufficient to warrant this assumption. Second, scrutiny of both our earlier membrane potential data at low concentrations in the presence of chlorides (Eisenman et al., 1977) and the lower concentration regions of the present data, where anion effects are expected to be least important, led to the conclusion that the principle factor contributing to the concentration dependence of P_{Tl}/P_K is the shift of the peak difference between Tl^+ and K^+ produced by Tl^+ loading (recall Fig. 9). In contrast, the

[4] These parameters are seen in Table III to be the products of binding constants of the anions in the presence of an x_o or y_o-loaded channel ($k_a^{x_o}, k_a^{y_o}$) and the ratios of the square roots of the appropriate rate constant · binding constant ($v \cdot k$) products defined in Table III. They reflect the shifts in energy peaks for the loading states indicated by the superscripts. For example, $v_{x_i}^{x_o x_o}$ designates the rate constant for transition of a species X^+ across a channel loaded with species X^+ on both outer sites; whereas $v_{x_i}^{x_o a x_o a}$ represents the rate constant for transition of the species X^+ across a channel loaded at both ends with species A^- as well as species X^+.

shift with K^+ loading of the energy difference between K^+ and Tl^+ peaks is small, as seen in the lower portion of Fig. 10, corresponding to the closeness to unity of the ratio $\beta_K/\gamma_K(= 1.12)$. This suggests that a principally electrostatic effect (seen on K^+ loading) shifts Tl^+ and K^+ peaks equally. It therefore seems reasonable to suppose that anion binding (also assumed to have a chiefly electrostatic effect on the Tl^+ and K^+ peaks) would also shift the Tl^+ and K^+ peaks almost equally. In this event θ_{xa} will equal ϕ_{xa}, both being given according to the definition of Table III, by

$$\theta_{xa} = \phi_{xa} = \tfrac{1}{2}K_{a(x)}\sqrt{\text{APS}} \tag{17}$$

where the APS, a parameter described in the text in relation to Eq. 2, is the bracketed portion of the physical definitions of θ_{xa} and ϕ_{xa}.

Fixing APS at a value of 2 from conductance measurements, we have the approximation

$$\theta_{xa} = \phi_{xa} = 0.707\,K_{a(x)} \tag{17a}$$

Only one free parameter remains with which to fit the potential data, namely the binding constant of the anion ($K_{a(x)}$) to the Tl^+-loaded channel. In this approximation Eq. 15 simplifies to:

$$\begin{aligned}
&\beta'_{xa} = \beta_x(1 + 0.707K_{a(x)}c'_a); \qquad \beta''_{xa} = \beta_x(1 + 0.707K_{a(x)}c''_a),\\
&\gamma'_{xa} = \gamma_x(1 + 0.707K_{a(x)}c'_a); \qquad \gamma''_{xa} = \gamma_x(1 + 0.707K_{a(x)}c''_a),\\
&\beta'_{ya} = \beta''_{ya} = \beta_y,\\
&\gamma'_{ya} = \gamma''_{ya} = \gamma_y.
\end{aligned} \tag{18}$$

The adequacy of these approximations can be seen from the fact that the experimental data generally fall between the solid curves in Fig. 7–10, corresponding to the indicated binding constants, and the dashed curves, corresponding to zero anion binding. Although it is not easy to distinguish the effects of one anion from another (partly owing to the relative insensitivity of the theoretical expressions for P_{Tl}/P_K to the effects of anion binding in the present approximation), the potential data on the average are rather well fit by an anion binding constant of the order of 10 M^{-1}, internally consistent with the values assessed from the individual channel conductances in single salts (recall Figs. 3 and 5). A value of this magnitude also produces the best fit to the single channel conductances in ionic mixtures (see Fig. 5 of Neher et al., 1978).

In further support of the postulated anion binding, we point out that all the above-described consequences of binding an anion near the channel mouth are consistent with the behavior of Appell et al.'s (1977) negatively charged gramicidin analogue, where the same concentration dependence of P_{Tl}/P_K is observed (but at almost 100 times lower concentrations) and the same approximate values for maximum limiting conductances when the effects of block are taken into account (Eisenman, Bamberg, and Läuger, unpublished data).

DISCUSSION

The Measured Binding Constants and Rate Constants for Li, Na, K, Rb, and Cs Depend on Ion Size in Systematic Ways that Suggest that the Binding and Translocation of the Group Ia Cations Is More Selective Than Has Previously Been Supposed.

Not only does our original 1B4S′ model (or the extended version in the zero anion binding limit) satisfactorily describe the conductance-concentration data for the group Ia cations, but, more importantly, the parameters extracted using it will here be seen in Fig. 11 to vary systematically, and in a physically reasonable way, with cation size. Fig. 11 summarizes the dependence on cation radius of the values of the experimentally determined binding constants (K^0, K^h, K^∞) and rate constants (G^0, G^h) extracted from the conductance data in Table I. For the 1B4S′ model, these phenomenological binding and rate constants can be directly interpreted in terms of the physical binding constants ($k_{x_o}, k_{x_i}^{x_o x_o}, k_{x_i}^{x_o x_o x_i}$) and rate constants ($v_i(k_{x_i}/k_{x_o}), v_{x_i}^{x_o x_o}$) of the model. For other situations, e.g. with the rate-determining barrier no longer assumed to be in the middle of the membrane, the physical parameters implied by the phenomenological constants will be different, as will be discussed in relation to Figs. 13 and 14. Here, we will describe the phenomenological binding and rate constants as if they actually corresponded to physical binding and rate constants, recognizing that for other models certain parameters, here called binding constants, may actually reflect only ratios of certain rate constants and that the rate-determining rate constants may correspond to quite different barriers in different models.

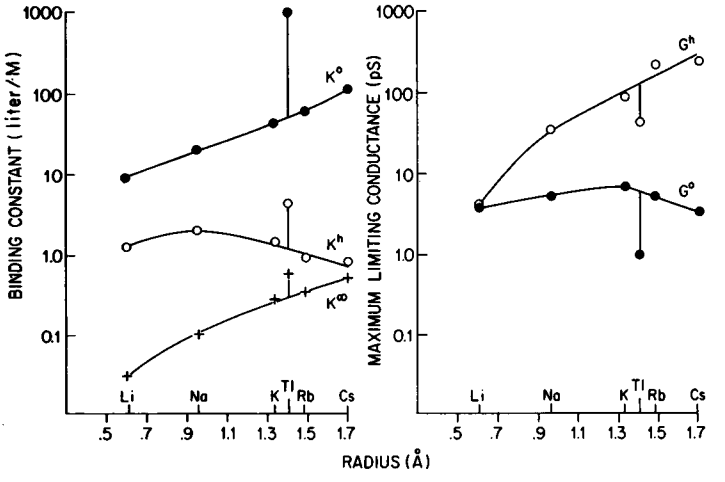

FIGURE 11 Regularities in the behavior of the individual values of phenomenological, "experimental" binding constants and rate constants calculated from the single channel conductance measurements for Li, Na, K, Rb, Cs, and Tl. K^0, K^h, K^∞, G^0, and G^h are plotted as a function of the Pauling crystal radius of the labeled cations.

Consider the group Ia cations first. The phenomenological binding constants K^0 and K^∞ can be seen to increase with the cation size (i.e. in the lyotropic sequence Cs Rb K Na Li), paralleling each other rather strikingly. These binding constants correspond in the 1B4S' model to the equilibrium processes of loading the outermost site of the empty channel and the last inner site of a loaded channel, respectively (recall the definitions in Table III). In contrast, the binding constant K^h is in the almost completely inverted Eisenman (1961) Sequence IX (Na>K>Li>Rb>Cs). This is the binding constant for the process of loading the first inner site of a channel both of whose outer sites are already loaded.

The behavior of the maximum limiting conductances (G^h and G^0), which correspond to the rate constant selectivity of the channel in the 1B4S' model, also vary systematically with cation size. Consistent with the traditional view (Haydon and Hladky, 1972; Läuger, 1973; Finkelstein, 1975), the values of conductance for all cations in the empty channel are very similar, as would be expected from their mobilities in a free aqueous solution. In contrast, the values of G^h for channels occupied by more than one cation differ by a factor (more than 20 between Li^+ and Cs^+) well above that expected from aqueous mobilities. The 1B4S' model seems to imply that once the gramicidin channel is loaded with more than one cation, diffusion within it can no longer be approximated by that characteristic of a simple aqueous solution.

Consider Tl^+ now. The extended 1B4S' model enabled us to allow for the complications due to anion binding and thus to extract out of the observed data the intrinsic binding constants and rate constants for Tl^+, independent of the anionic salt studies. These intrinsic parameters are given in Table II; and the "best" values of these are plotted in Fig. 11 at the radius of Tl^+, which lies between that for K^+ and Rb^+. Looking at the binding constant selectivity first, it is clear that this ion is "supra Ia" compared to a like-sized group Ia cation (Eisenman and Krasne, 1973) for all three loading states. Conversely, looking at the maximum limiting conductances, it is "sub Ia" for all conductance states. These two findings in the 1B4S' model would imply that Tl^+ sees both a deeper well and a higher barrier than does a comparably sized group Ia cation. In addition, since the relative selectivity of Tl^+ is sensitive to ligand type (Eisenman and Krasne, 1973), the finding that Tl^+ is supra Ia for K^0, K^h, and K^∞ (and sub Ia for G^0 and G^h) would be consistent with the view that the same kinds of ligands are involved in Tl^+ binding at all sites. This supports the notion that such ligands are intrinsic to the channel, rather than associated with some special structures at the channel mouth.

Not only are the trends in the individual binding constants and rate constants regular; but the product $(G^0 \cdot K^0)$ also behaves as expected phenomenologically from the discussion of Fig. 2, as well as in the way demanded theoretically for the 1B4S' model (Sandblom, et al., 1977). In particular, this product should correspond to the limiting value of the permeability at low salt concentration. Therefore, the ratios of this product between different cations should agree with the appropriate values of the permeability ratio measured by potential. That this is indeed the case is clearly demonstrated in Fig. 12, where this comparison has been carried out for the indicated pairs of

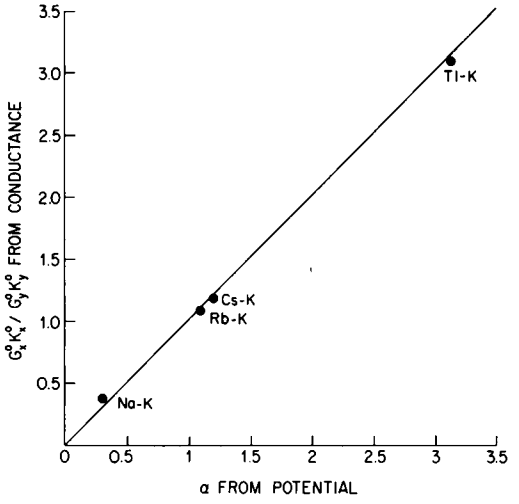

FIGURE 12 Verification that the low concentration conductances in single salts agree with the permeability ratios measured in the low concentration limit. The ordinate plots the conductance ratios ($G^0_x K^0_x / G^0_x K^0_x$) from Tables I and II. The abscissa plots the corresponding values of the limiting permeability ratios ($P_x/P_K)_{c\to 0} = \alpha$), which are as follows: P_{Tl}/P_K = 3.25 (Table IV), P_{Na}/P_K = 0.33 (Eisenman et al. 1976*a*, Table III), P_{Cs}/P_K = 1.18 (Eisenman, 1978, Fig. 12), P_{Rb}/P_K = 1.07 (Eisenman, unpublished). Our values for P_{Cs}/P_K, P_{Na}/P_K agree with values of P_{Cs}/P_K = 1.31; P_{Rb}/P_K = 1.03, and P_{Na}/P_K = 0.29 calculated from Myers and Haydon's (1972) bi-ionic values of P_{Cs}/P_{Na}, P_{Rb}/P_{Na}, and P_K/P_{Na} at 0.1 M.

ions. Note that for other models, for example when the rate-determining step occurs at the entrance to the channel instead of at its midpoint, the x-intercept would correspond to different processes, as will be discussed at the end of this section.

Energy Diagram for the Effect of Loading Cations and Anions on the Energy Wells and Peaks Governing Cation Permeation

The data obtained to this point are sufficient to define, within the context of the 1B4S′ model, the energy profile governing cation permeation, and the shifts of this profile on binding various cation and anion species. Fig. 13 presents such an energy level diagram for Tl^+ for the states of loading indicated along the abscissa, using the "best" Tl^+ data of Table II and expressing all K's in concentration-independent mole fraction units by multiplying by 55.5 mol/liter of water. (For our model where all concentration dependences in the data are incorporated in the values of the concentration-independent binding- and rate-constants, *all* sources of energy change are included in the Free Energies, which therefore include, among other terms, the conformational energy of the gramicidin molecule, the hydration state of the channel, and any volume changes in the channel under various conditions of loading).

We will discuss the construction of Fig. 13 in detail because this will enable the reader to see most clearly the interconnections between the somewhat abstract parameters and their more concrete representation as energies. Consider first the state for a Tl^+ interacting with a completely empty channel (0 0 — —). The level of the energy

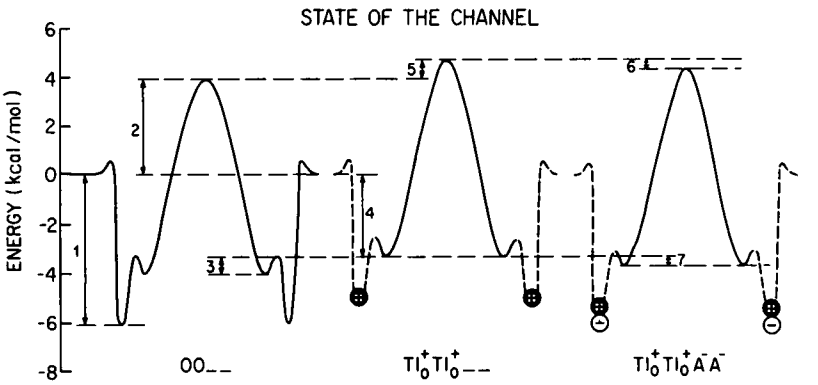

FIGURE 13 Reconstruction for the 1B4S' model of the energy levels seen by Tl^+ in crossing the gramicidin A channel under the conditions of loading labeled along the abscissa. Three states are indicated. At the left, an empty channel; in the middle, a channel whose outermost sites are loaded by Tl^+ cations; and at the right, a channel whose outermost sites are loaded by Tl^+ cations as well as secondarily bound anions. Solid lines are used to indicate available energy wells and peaks. Dashed lines are used to indicate loaded sites, further occupancy of which is not permitted.

well for the strongest binding site (the outer site in the 1B4S' model) is given by the energy of that well relative to the aqueous solution, as indicated by the distance (1). For the 1B4S' model, by recalling the definitions of Table III, the magnitude of this energy is $-RT \ln (K^0_{Tl}/2)$ or -6.12 kcal/mol ($-10.3\ RT$). The height of the peak relative to aqueous solution (2) is given by $RT \ln (A/G^0_x K^0_x)$, where A is the frequency factor in the Eyring rate theory ($6.21 \times 10^{12} s^{-1}$). This height is 3.95 kcal/mol (6.7 RT). The barrier height of the central peak above the well of the first binding site is, of course given by (2)–(1) and is 10.1 kcal/mol (17 RT). Lastly, for the empty channel, the level of the well corresponding to the inner site will be estimated below as a shift from the level, which we will now calculate in the middle diagram when both outer sites are loaded.

We next consider the state ($Tl_o^+ Tl_o^+$ — —) in the middle diagram where both outer sites are loaded by Tl^+. The solid line indicates the energy profile for loading an additional cation (the dashed lines merely indicating visually the loaded, and therefore no longer occupiable, outer wells). In this case the level of the inner well relative to the aqueous phase (4) is given by $-RT \ln K^h_x$ or -3.3 kcal/mol ($-5.6\ RT$). The height of the central peak can be calculated from the peak shift (5) in two alternative ways, permitting a consistency check. Using conductance data only, this shift is given by $RT \ln (G^0_x K^0_x / G^h_x K^h_x$ or 0.7 kcal/mol (1.2 RT). The alternative estimate of this shift for the 1B4S' model is based upon a combination of the potential data of Table IV, together with the conductance data of Table II. (The peak shift (5) is then given by $RT \ln (K^0_x/2\beta_x)^2$ or 0.5 kcal/mol (0.9 RT), which is not bad agreement).

We are now in a position to estimate the energy level of the inner site of the empty channel for the left-hand diagram. We do this by assuming that the well shift (3) is

TABLE IV

"EXPERIMENTAL" PARAMETERS DEFINING P_{Tl}/P_K IN THE APPROXIMATION, EQ. 18, OF THE EXTENDED 1B4S' THEORY, TO WHICH THEORETICAL CURVES HAVE BEEN DRAWN

α	β_{Tl}	γ_{Tl}	β_K	γ_K	$K_{a(Tl)}$
3.25	350.*	80.*	16.*	14.*	0.10*

*M^{-1}.

the same or a little larger than the peak shift (5), according to which the level of the inner site in the left-hand diagram has been drawn. Notice that the level of this well relative to the outer is intuitively reasonable (recall Fig. 1) and is consistent with the assumption (Sandblom et al. 1977) that the binding to the outer site is stronger than binding to the inner site for a 1B4S' model.

We finally examine on the right-hand diagram the effect of loading an anion onto a Tl^+-loaded channel (corresponding to the state $Tl_o^+ Tl_o^+ A^- A^-$). The anionic peak shift (6) produced by anion binding is given directly as $-RT$ ln (APS). This is -0.4 kCal/mol ($-0.7\,RT$). An alternative estimate of this is given from the potential data of Table IV as $-RT \ln (K_{a(x)}/2\theta_{xa})^2$. Recalling Eq. 17, this reduces to the same (internally consistent) value of $-RT$ ln (APS). The shift in level of the inner binding site (7) is given from the anionic well shift by $-RT$ ln (AWS), -0.4 kCal/mol ($-0.7\,RT$), a value of course identical to the peak shift (6) in the approximation (APS = AWS) used in Table IV, suggested by our experimental results.

A very important feature of the energy profile in Fig. 13 is how much lower the well of the outer site (and even of the inner site) is relative to the reference aqueous solution. That these are lower than in aqueous solution must reflect specific interactions with the amide carbonyl ligands of the gramicidin channel, which must be stronger than the energies of interaction with the water molecules that they replace. Such strong interactions are consistent with the known fact that the enthalpies of solvation in typical amide solvents are higher than those for water (see Eisenman and Krasne, 1973, Fig. 2.4). Although such interactions must provide the basis for understanding the high observed conductance of a gramicidin A channel, as correctly suggested by Finkelstein and Parsegian (Finkelstein, 1975; cf. Parsegian, 1969), these interactions must lower the height of the peak in addition to the depth of the well, since it is the peak-well difference (i.e. the barrier height) that determines the value of the rate constant corresponding to the maximum limiting conductance. Incidentally, as will be pointed out in the following section, it seems likely that for the high conductance (corresponding to G^h), it is indeed the central barrier that is rate determining, so that the present model is applicable even though at low concentrations the rate-determining barrier (G^0) appears to be at the mouth of the channel. It is important to realize that the energy level of the well corresponding to K^0 is the same, regardless of where the barrier is.

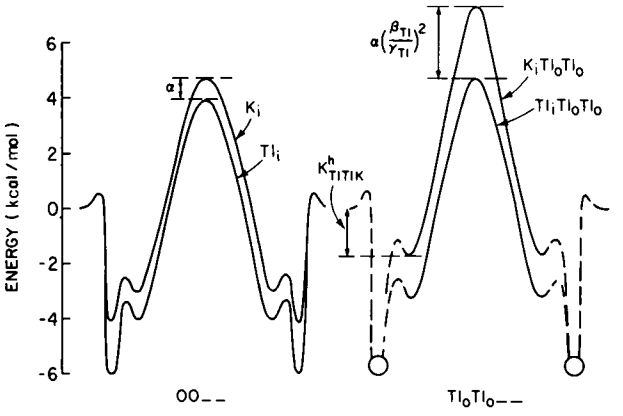

FIGURE 14 Comparison of the energy level diagram for K^+ and Tl^+. The left-hand figure compares the energies seen by K^+ ions or Tl^+ ions (labeled K_i and Tl_i on the figure) as they cross the empty channel (at the left), as well as for the peak shift for these species in a Tl^+-loaded channel (at the right). The peak energy difference intrinsic to the empty channel is given by $kT \ln \alpha$; whereas the peak energy difference for the Tl^+-loaded channel is $kT \ln \alpha(\beta_{Tl}/\gamma_{Tl})^2$ (cf. Eisenman et al., 1977, Fig. 13; and Sandblom et al., 1977, Fig. 4). As in Fig. 13, dashed lines are used to indicate loaded sites, further occupancy of which is not permitted.

The profile for Tl^+ is not atypical of that for the more usual cations. A reconstruction for K^+, carried out in the same way as for Tl^+, is given in Fig. 14 (left), where the wells can be seen also to lie substantially below the aqueous reference level. For completeness, the right-hand side of Fig. 14 also illustrates the shift in the energy peaks governing K^+ and Tl^+ permeation on loading the outer sites of the channel with Tl^+.

A characterization of the rate constants, binding constants, and energy profiles like the above, but in terms of the most realistic model for the gramicidin channel, is a necessary prerequisite for a future interpretation at a more molecular level, which would then be carried out by considering the extent to which the individual contributions of, for example, electrostatic interactions, changes in conformational energies, changes in hydration, etc. could produce the proper energy levels for different states. We emphasize that the present model makes no restrictive assumptions on the kinds of interactions that could give rise to the different energy levels other than to assume that *all* interactions (ion-ion, ion-channel, ion-water, water-channel, channel-lipid, etc.) as well as any conformational rearrangements can be represented by the energy levels of the finite number of states of the model.

Alternative Physical Interpretations of the Single-Channel Conductance Data if the Central Barrier Is Not the Only Rate-Determining Step

As mentioned in the Introduction, the recent experimental demonstration by Schagina, Grinfeldt, and Lev of pairwise movement of Rb^+ ions at low salt concentrations indicates that the assumption we have made in all our work so far, that the central barrier was rate determining, cannot be true at low concentrations. There is, however, nothing to indicate that the central barrier is not rate-determining at high concentrations; and,

indeed, such a central rate-determining barrier would be consistent with the "hyperbolic" conductance-voltage characteristic at high concentrations, as well as with the occurrence of a maximum in the conductance at these concentrations. It seems likely, therefore, that the present 1B4S' model represents the appropriate high concentration limit of a more general 3B4S' (or 3B4S") model that would be needed to account for the data at low concentrations. To reinterpret the low salt concentration parameters one then needs to assume that the central barrier in Fig. 14 is much smaller and then to recalculate the heights of the rate-determining steps in terms of the rate constant for jumping into the solution out of the energy well in Figs. 13 or 14 corresponding to the strongest binding site in the channel. The peak determining the low concentration permeability also has a simple meaning in this case, corresponding in the 3B4S' model to the product of the binding constant of the first site and its unloading rate constant into the aqueous solution (this product is simply the forward rate constant for loading the first site in the channel). Such a revised profile at low concentrations will also be consistent with the well-known "saturating" conductance-voltage characteristic at low concentrations. Whether or not models with three-barriers and two-sites (Hladky et al., 1978) are sufficient, or whether four-sites are demanded by the data is presently controversial. These alternatives are distinguishable by comparing their expectations for the concentration dependences of unidirectional flux ratio, conductance, and shape of the conductance-voltage characteristic for single salts, as well as the permeability ratio extracted from membrane potentials in mixtures of several cations. We believe, as a result of work now being carried out in collaboration with Hägglund and Enos, which explores Heckmann-Chizmadjev-Eyring type single-filing models with two or three barriers and two or four sites, that a really satisfactory model must belong to the class three-barrier, four-sites (Hägglund et al., 1978). Previous models like Sandblom et al.'s (1978) one-barrier, four-site model and Hladky's (1972) three-barrier, two-site models would then be interesting special cases, representing high and low concentration limits, respectively, for gramicidin, but perhaps in their own right representing other channels quite adequately.

We wish to thank Sally Krasne, Jarl Hägglund, Bruce Enos, and Sergio Ciani for reading the manuscript and making valuable comments.

This work has been carried out under the generous support of the National Science Foundation (Grants GB 30835 and PCM 7620605) and the U.S. Public Health Services (NS 09931), as well as the Swedish Medical Research Council (04138).

Received for publication 12 October 1977 and in revised form 17 January 1978.

REFERENCES

ANDERSEN, O. S. 1975. Ion-specificity of gramicidin channels. International Biophysics Congress, Copenhagen, Denmark. 112. (Abstr.).

ANDERSEN, O. S. 1978. Ion transport across simple membranes. *In* Renal Function. G. H. Giebisch and E. Purcell, editors. Independent Publishers Group, Port Washington, N.Y. 71–99.

APELL, H.-J., E. BAMBERG, H. ALPES, and P. LÄUGER. 1977. Formation of ion channels by a negatively charged analog of gramicidin A. *J. Membr. Biol.* **31**:171.

BAMBERG, E., K. NODA, E. GROSS, and P. LÄUGER. 1976. Single-channel parameters of gramicidin A, B and C. *Biochim. Biophys. Acta.* **419**:223.

BULL, H. B. 1964. An Introduction to Physical Biochemistry. F. A. Davis Company, Philadelphia, Pa. 120.

CAHALAN, M., and T. BEGENISICH. 1976. Sodium channel selectivity. Dependence on internal permeant ion concentration. *J. Gen. Physiol.* **68**:11.

CHIZMADJEV, Y. A., and S. K. AITYAN. 1974. Theory of ion transport through selective channels of biological membranes. First Winter School on Biophysics of Membrane Transport. Poland:Szklarska Poreba. Privately printed. 46–134.

CHIZMADJEV, Y. A. and S. K. AITYAN. 1977. Ion transport across sodium channels in biological membranes. *J. Theor. Biol.* **64**:429.

EISENMAN, G. 1961. On the elementary atomic origin of equilibrium ionic specificity. *In* Symposium on Membrane Transport and Metabolism. A Kleinzeller and A. Kotyk, editors. Academic Press, Inc., New York. 163.

EISENMAN, G. 1978. New developments in selectivity: neutral peptide and peptide-like carriers and channels in lipid bilayers. Proceedings of the Conference on Ion-Selective Electrodes. E. Pungor, editor. Publishing House of Hungarian Academy of Sciences, Budapest, Hungary. In press.

EISENMAN, G., and S. KRASNE. 1973. The ion selectivity of carrier molecules, membranes, and enzymes. *In* MTP International Review of Science, Biochemistry Series, Vol. 2, C. F. Fox, editor. Butterworth & Co., (Publishers) Ltd., 27.

EISENMAN, G., S. KRASNE, and S. CIANI. 1976*a*. Further studies on ion selectivity. *In* Ion and Enzyme Electrodes in Biology and Medicine. M. Kessler, L. Clark, D. Lübbers, I. Silver, and W. Simon, editors. Urban & Schwarzenberg, Munich, W. Germany. 3.

EISENMAN, G., J. SANDBLOM, and E. NEHER. 1976*b*. Evidence for multiple occupancy of gramicidin A channels by ions. *Biophys. J.* **16**:81*a*. (Abstr.).

EISENMAN, G., J. SANDBLOM, and E. NEHER. 1977. Ionic selectivity, saturation, binding and block in the gramicidin A channel: A preliminary report. *In* ninth Jerusalem Symposium on Metal-Ligand Interactions in Organic and Biochemistry. Part 2. D. Reidel Publishing Company, Dordrecht-Holland. 1.

FINKELSTEIN, A. 1975. Discussion paper. *Ann. N.Y. Acad. Sci.* **264**:244.

GRELL, E. 1975. Structure and dynamic properties of ion-specific antibiotics. *In* Membranes–A Series of Advances, Vol. 3. G. Eisenman, editor. Marcel Dekker, New York. 1.

HAGIWARA, S., and K. TAKAHASHI. 1974. The anolomous rectification and cation selectivity of the membrane of a starfish egg cell. *J. Membr. Biol.* **18**:61.

HÄGGLUND, J., J. SANDBLOM, B. ENOS, and G. EISENMAN. 1978. Single-filing multi-barrier models for gramicidin channels. *Biophys. J.* **21**:26*a* (Abstr.).

HECKMANN, K. 1972. Single file diffusion. *In* Biomembranes. F. Kreuzer and J. F. G. Slegers, editors. Vol. 3, Plenum Publishing Corp., New York. 127.

HECKMANN, K., and Z. VOLLMERHAUS. 1970. Zur theorie der "single file"-diffusion. IV. Vergleich von Leerstellendiffusion und "knock-on"-Mechanismus. *Phys. Chem. (NF).* **71**:320.

HECKMANN, K., B. LINDEMANN, and J. S. SCHNAKENBERG. 1972. Current-voltage curves of porous membranes in the presence of pore-blocking ions. I. Narrow pores containing no more than one moving ion. *Biophys. J.* **12**:683.

HILLE, B. 1975. Ionic selectivity of Na and K channels of nerve membranes. *In* Membranes—A Series of Advances, Vol. 3. G. Eisenman, editor. Marcel Dekker, Inc., New York. 255.

HLADKY, S. B. 1972. The two-site lattice made for the pore. Appendix B', Ph. D. Dissertation, Cambridge University, England.

HLADKY, S. B., and D. A. HAYDON. 1970. Discreteness of conductance change in bimolecular lipid membranes in the presence of certain antibiotics. *Nature (Lond.).* **225**:451.

HLADKY, S. B., and D. A. HAYDON. 1972. Ion transfer across lipid membranes in the presence of gramidicin A. I. Studies of the unit conductance channel. *Biochim. Biophys. Acta.* **274**:294.

HLADKY, S. B., B. W. URBAN, and D. A. HAYDON. 1978. Ion movements in pores formed by gramicidin A. *In* Membrane Transport Processes. Vol. 3. C. Stevens, R. Tsien and W. Chandler, editors. Raven Press, New York. In press.

HODGKIN, A. L., and R. D. KEYNES. 1955. The potassium permeability of a giant nerve fiber. *J. Physiol. (Lond.).* **128**:61.

KRASNE, S., and G. EISENMAN. 1976. Influence of molecular variations of ionophore and lipid on the se-

lective ion permeability of membranes: I. Tetranactin and the methylation of nonactin-type carriers. *J. Membr. Biol.* **30**:1.

LÄUGER, P. 1973. Ion transport through pores: A rate-theory analysis. *Biochim. Biophys. Acta.* **311**:423.

LEVITT. D. G. 1978. Electrostatic calculations for an ion channel. II. Kinetic behavior of the gramicidin A channel. *Biophys. J.* **22**:000.

MYERS, V. B., and D. A. HAYDON. 1972. Ion transfer across lipid membranes in the presence of gramicidin A. II. The ion selectivity. *Biochim. Biophys. Acta.* **274**:313.

NEHER, E. 1975. Ionic specificity of the gramicidin channel and the thallous ion. *Biochim. Biophys. Acta.* **401**:540.

NEHER, E., J. SANDBLOM, and G. EISENMAN. 1978. Ionic selectivity, saturation and block in gramicidin A channels. II. Saturation behavior of single channel conductances and evidence for the existence of multiple binding sites in the channel. *J. Membr. Biol.* In press.

PARSEGIAN, A. 1969. Energy of an ion crossing a low dielectric membrane. Solutions to four relevant electrostatic problems. *Nature (Lond.).* **221**:844.

SANDBLOM, J., G. EISENMAN, and E. NEHER. 1977. Ionic selectivity, saturation and block in gramicidin A channels. I. Theory for the electrical properties of ion selective channels having two pairs of binding sites and multiple conductance states. *J. Membr. Biol.* **31**:383.

SZABO, G., G. EISENMAN, and S. CIANI. 1969. The effects of the macrotetralide actin antibiotics on the electrical properties of phospholipid bilayer membranes. *J. Membr. Biol.* **1**:346.

URRY, D. W., M. C. GOODALL, I. D. GLICKSON, and D. C. MAYERS. 1971. The gramicidin A transmembrane channel: Characteristics of head-to-head dimerized $\pi_{(L,D)}$ helices. *Proc. Natl. Acad. Sci. U.S.A.* **68**:1907.

ZEFFREN, E., and P. L. HALL. 1973. The Study of Enzyme Mechanisms. John Wiley and Sons, Inc., New York. 67.